Induction of pathogenic TH17 cells by inducible salt-sensing kinase SGK1

Citation: Wu, Chuan, Nir Yosef, Theresa Thalhamer, Chen Zhu, Sheng Xiao, Yasuhiro Kishi, Aviv Regev, and Vijay K. Kuchroo. "Induction of pathogenic TH17 cells by inducible salt-sensing kinase SGK1." Nature 496, no. 7446 (March 6, 2013): 513-517.

As Published: http://dx.doi.org/10.1038/nature11984

Publisher: Nature Publishing Group

Persistent URL: http://hdl.handle.net/1721.1/80822

Version: Author's final manuscript: final author's manuscript post peer review, without publisher's formatting or copy editing

Induction of pathogenic Th17 cells by inducible salt sensing kinase SGK1

Chuan Wu[1,4], Nir Yosef[1,2,4], Theresa Thalhamer[1,4], Chen Zhu[1], Sheng Xiao[1], Yasuhiro Kishi[1], Aviv Regev[2,3,#], Vijay Kuchroo[1,2,#]

[1] Center for Neurologic Diseases, Brigham and Women's Hospital, Harvard Medical School, Boston, MA 02115

[2] Broad Institute of MIT and Harvard, 7 Cambridge Center, Cambridge, Massachusetts 02142

[3] Howard Hughes Medical Institute, Department of Biology, Massachusetts Institute of Technology, Cambridge, Massachusetts 02140

[4] These authors contributed equally to this study.

to whom correspondence should be addressed: aregev@broad.mit.edu (AR), vkuchroo@rics.bwh.harvard.edu (VK):

Th17 cells are highly proinflammatory cells critical for clearing extracellular pathogens and for induction of multiple autoimmune diseases[1]. IL-23 plays a critical role in stabilizing and reinforcing the Th17 phenotype by increasing expression of IL-23 receptor (IL-23R)[3] and endowing Th17 cells with pathogenic effector functions[2]. However, the precise molecular mechanism by which IL-23 sustains the Th17 response and induces pathogenic effector functions has not been elucidated. Here, we used transcriptional profiling of developing Th17 cells to construct a model of their signaling network and nominate major nodes that regulate Th17 development. We identified serum glucocorticoid kinase-1 (SGK1), a serine-threonine kinase[4], as an essential node downstream of IL-23 signaling. SGK1 is critical for regulating IL-23R expression and stabilizing the Th17 cell phenotype by deactivation of Foxo1, a direct repressor of IL-23R expression. SGK1 has been shown to govern Na^+ transport and salt (NaCl) homeostasis in other cells[5, 6,7, 8]. We here show that a modest increase in salt concentration induces SGK1 expression, promotes IL-23R expression and enhances Th17 cell differentiation *in vitro* and *in vivo*, accelerating the development of autoimmunity. Loss of SGK1 abrogated Na^+-mediated Th17 differentiation in an IL-23-dependent manner. These data demonstrate that SGK-1 plays a critical role in the induction of pathogenic Th17 cells and provides a molecular insight into a mechanism by which an environmental factor such as a high salt diet triggers Th17 development and promotes tissue inflammation.

Main text

To determine the molecular mechanisms by which naïve T cells develop into effector Th17 cells, we measured genome-wide mRNA expression profiles using microarrays along 18 time points over 72 hours following the *in vitro* exposure of naive T cells to Th17 polarizing conditions (TGF-β1 with IL-6). To examine the role of IL-23 in Th17 development, we added IL-23 at the late time points (48 – 72 h) and monitored the transcriptional response in both wild-type (WT) and *Il23r*$^{-/-}$ cells. We ranked the genes according to their extent of induction in cells treated with TGF-β1 and IL-6 (relative to nonpolarized activated T cells) and repression in *Il23r*$^{-/-}$ cells (relative to WT cells) (**Methods**; **Fig. 1a** and **Supplementary Table 1**). SGK1 was one of the top ranking genes, whose transcriptional regulation is strongly associated with both IL-23R signaling and Th17 cell differentiation (**Fig. 1a**). qPCR analysis showed that SGK1 is induced at low levels by TGF-β1 (iTreg), and not induced in other T cell subsets (Th0, Th1, Th2). As expected, it is most highly expressed under Th17 differentiation conditions (**Fig. 1b**). SGK1 expression is strongly induced during the first two hours following stimulation of naïve T cells under Th17-polarizing conditions. This is followed by a sharp decline by 10 hours to a steady expression level that is still substantially higher than in the control population (**Fig. 1c** and **Supplementary Fig. 1a**). Furthermore, expression of SGK1 is specifically induced and maintained by exposure to IL-23 (**Fig. 1c** and **Supplementary Fig. 1b**). While *Il23r*$^{-/-}$ T cells initially produce SGK1 mRNA, they cannot sustain this expression (**Supplementary Fig. 1b, c**). Finally, the kinase activity of SGK1 is also significantly higher in Th17 cells than in other T cell subsets (**Supplementary Fig. 1d**),

and restimulation of differentiated Th17 cells with IL-23 further elevates SGK1 kinase activity (**Supplementary Fig. 1e**). Thus, IL-23 signaling is critical for maintaining SGK1 expression during Th17 cell differentiation.

Network analysis[9] of the transcriptional changes in *Il23r*$^{-/-}$ T cells singled out SGK1 as a potential nodal point downstream of IL-23R signaling. Based on a curated database of protein-protein interactions (PPI), we constructed a network model that connects known proteins of the IL-23R signaling pathway (see **Methods**) to the transcription factors whose function is dysregulated in *Il23r*$^{-/-}$ cells (**Methods**; **Fig. 1d** and **Supplementary Fig. 1f**). We ranked the network's nodes based on a centrality measure, defined as the fraction of IL-23R-affected transcription factors downstream of that node in the network (**Methods**; **Supplementary Table 1**). SGK1 was the highest-ranking node (**Supplementary Fig. 1g**), suggesting that it acts both as a transcriptional target of IL-23R signaling and as a kinase that may mediate the transcriptional effects of the pathway.

Using *Sgk1*$^{-/-}$ mice, we studied the impact of loss of SGK1 on Th17 differentiation *in vitro*. We observed no abnormality of SGK1-deficient T cells during primary differentiation into Th17 cells (**Fig. 1e**). However, *Sgk1*$^{-/-}$ Th17 cells restimulated with IL-23 showed impaired IL-17 production (**Fig. 1e** and **Supplementary Fig. 2b**). Memory *Sgk1*$^{-/-}$ T cells also showed a defect in IL-17 production upon IL-23 stimulation, but not under stimulation with TGF-β1 and IL-6 (**Supplementary Fig. 2a**). To study the function of SGK1 specifically in IL-17-producing CD4^{+} T cells, we generated *Il17f*^{Cre}*Sgk1*$^{fl/fl}$ mice.

Il17f^{Cre}*Sgk1*$^{fl/fl}$ T cells also showed no defect in primary Th17 differentiation, but displayed reduced IL-17 production upon restimulation with IL-23 (**Fig. 1f** and **Supplementary Fig. 2c**). Further, IL-23R expression was also significantly reduced in *Sgk1*$^{-/-}$ T cells (**Fig. 1g**). Thus, loss of SGK1 does not affect primary Th17 differentiation, but profoundly affects their stability and IL-23R expression. One possible explanation for the dispensability of SGK1 during primary Th17 differentiation is redundancy with other kinases, such as its homolog AKT[10]. However, SGK1 seems to be indispensable for IL-23R-dependent stability and maintenance of Th17 cells.

Microarray analysis of *Sgk1*$^{-/-}$ vs. WT Th17 cells restimulated with IL-23 showed a significant overlap in differentially expressed genes with the *Il23r*$^{-/-}$ vs. WT IL-23-restimulated Th17 cell profiles, further supporting the functional relatedness of the SGK1 and IL-23R pathways (Fisher exact test, $p<10^{-3}$) (**Fig. 1h** and **Supplementary Fig. 2d**). Consistently, genes downregulated in *Sgk1*$^{-/-}$ cells are significantly enriched (Fisher exact test, $p<10^{-6}$) for genes that are upregulated in WT Th17 cells compared to other T cell subsets[11] (**Methods** and **Supplementary Fig. 2e**), Selected genes were confirmed by qPCR analysis (**Supplementary Fig. 2f**). Genes from several other pathways, including cell cycle and proliferation, which may be related to the known role of SGK1 as a regulator of proliferation and apoptosis[7, 8, 10], are also enriched (over- or underexpressed) (**Supplementary Table 2**). Although our analysis strongly associates SGK1 with the Th17 program, genes important for development and function of other T cell subsets, such as *Ifng*, *Tbx21* or *Gata3* were also dysregulated in *Sgk1*$^{-/-}$ cells, suggesting possible additional effects of this kinase in other T cell subsets.

To determine the role of SGK1 *in vivo*, we immunized *Cd4*^{Cre}*Sgk1*$^{fl/fl}$ mice with MOG_{35-55} to induce experimental autoimmune encephalomyelitis (EAE). SGK1-deficient mice exhibited significantly reduced EAE incidence and severity. IL-17 production from infiltrated $CD4^+$ T cells in different organs of SGK1-deficient mice was also reduced, whereas IFN-γ levels were unaffected (**Fig. 2a** and **Supplementary Fig. 3a**). When we restimulated the isolated T cells from immunized mice with IL-23 in the presence of MOG_{35-55}, the SGK1-deficient T cells also exhibited impaired IL-17 but normal IFN-γ production (**Supplementary Fig. 3b, c**). Next, using *Il23r*^{gfp} reporter mice, we observed reduced IL-23R (GFP) expression on infiltrating $CD4^+$ T cells in different organs of SGK1-deficient mice undergoing EAE (**Supplementary Fig. 4a**). Consistent with *Cd4*^{Cre}*Sgk1*$^{fl/fl}$ mice, reduced Th17 differentiation and disease severity were also observed in *Il17f*^{Cre}*Sgk1*$^{fl/fl}$ mice during EAE (**Fig. 2b**). In addition, to exclude any effects of SGK1-deficient bystander cells, we transferred purified *Il17f*^{Cre}*Sgk1*$^{fl/fl}$ $CD4^+$ T cells into *Rag2*$^{-/-}$ mice and induced EAE. Mice which had received SGK1-deficient T cells developed attenuated disease as compared to mice received WT T cells (**Supplementary Fig. 4b**).

To determine why we observed fewer Th17 cells in SGK1-deficient mice, we transferred purified GFP^+ cells from differentiated *Cd4*^{Cre}*Sgk1*$^{fl/fl}$*Il17a*^{gfp} or control Th17 cells to congenic Ly5.1 mice and traced the IL-17 GFP^+ cells in different organs following immunization with MOG_{35-55} (**Fig. 2c**). Starting with the same number of $CD4^+$IL-17^+ T cells, we found that 7 and 12 days after transfer, SGK1-deficient Th17 cells failed to

maintain IL-17 production, especially in the central nervous system (CNS) (**Fig. 2d** and **Supplementary Fig. 4c**). Next, we crossed *Il17f*^{Cre}*R26R*^{eYFP} mice onto the SGK1-deficient background, and analyzed the expression of IL-17 in T cells that had turned on the *Il17f* gene as determined by eYFP-expression. We induced EAE in these mice and analyzed the frequency of eYFP^{+} cells producing IL-17 in infiltrating CD4^{+} T cells in the lymph nodes (LN) and CNS. The *Sgk1*$^{-/-}$ reporter mice exhibited a smaller proportion of CD4^{+}eYFP^{+} T cells in both organs. Furthermore, there was a dramatic loss of IL-17 expression by eYFP^{+} T cells in the SGK1-deficient mice, indicating that Th17 cells could not stably retain IL-17 production during EAE (**Fig. 2e** and **Supplementary Fig. 4d**).

To better understand the role of SGK1 in Th17 cells, we conducted another network analysis, using PPI data to connect SGK1 to the transcription factors whose activity is dysregulated in *Sgk1*$^{-/-}$ Th17 cells (**Methods**). The analysis suggested Foxo1 as one of the highest-ranking nodes downstream of SGK1 (**Fig. 3a**; **Supplementary Table 1** and **Supplementary Fig. 5a**). Foxo1 phosphorylation by SGK1 has previously been shown in adipocytes to lead to its deactivation and translocation from the nucleus to the cytoplasm[12]. Consistently, we have observed that SGK1 phosphorylates Foxo1 **(Supplementary Fig. 5b)**. By immunoblot of *Sgk1*$^{-/-}$ Th17 cells restimulated with IL-23, we confirmed that not only is there reduced phosphorylation of Foxo1 in the nucleus, but there was increased mRNA and protein expression of Foxo1 (**Fig. 3b, c**), suggesting that compromised phosphorylation of Foxo1 can result in its own transcriptional upregulation. It has been previously shown that Foxo1 can regulate its own expression[13] and we have

found that Foxo1 binds to a site located about 1 kilobase (kb) upstream of the first exon in the *Foxo1* locus (**Supplementary Fig. 6a**). Transfection of a *Foxo1* luciferase reporter in the presence of Foxo1 led to increased luciferase activity (**Supplementary Fig. 6b)**, while increasing expression of SGK1 in the presence of Foxo1 resulted in a dose-dependent decrease in reporter activity, suggesting that SGK1 inhibited Foxo1-mediated transactivation of its own promoter (**Fig. 3d**).

To decipher the consequences of Foxo1 expression on Th17 cell development, we used *Foxo1*$^{-/-}$ CD4^{+} memory T cells and observed increased expression of IL-23R and IL-17A compared to WT cells, indicating that Foxo1 may act as a repressor of Th17 cell development and of IL-23 signaling (**Fig. 3e** and **Supplementary Fig. 6c**). We also found potential binding sites of Foxo1 located about 1 kb upstream of the first exon of the *Il23r* locus by ChIP-PCR (**Supplementary Fig. 6d**). Moreover, there is significantly enriched binding of Foxo1 on the *Il23r* promoter region in *Sgk1*$^{-/-}$ cells compared to WT T cells, indicating enhanced suppression of *Il23r* transcription in the absence of SGK1 (**Fig. 3f**). RORγt has been suggested to be the master transcription factor of Th17 development and ChIP-seq[28] and our ChIP-PCR analysis confirmed that IL-23R is one of the targets of RORγt (**Supplementary Fig. 6e**). Indeed, we observed that the *Il23r* promoter is transactivated by RORγt in IL-23-restimulated Th17 cells and it can be inhibited by Foxo1 in a dose-dependent manner (**Supplementary Fig. 6f, g**). While Foxo1 inhibited RORγt-mediated *Il23r* expression, co-expression of SGK1 together with RORγt and Foxo1 abrogated the suppressive effects of Foxo1 and rescued *Il23r* promoter transcriptional activity (**Fig. 3g**). Additionally, the inhibition of *Il23r* transcription by a

phosphorylation-insensitive triple alanine mutant of Foxo1, Foxo1 AAA, was not reduced in the presence of SGK1 (**Supplementary Fig. 6h**). Furthermore, we observed an endogenous Foxo1-RORγt interaction in primary Th17 cells (**Fig. 3h**). These data support a model whereby some of the effects of SGK1 are due to phosphorylation of Foxo1, which may be a key step in relieving RORγt from Foxo1-mediated inhibition, enhancing the expression of IL-23R.

SGK1 has been reported to act as a mediator for sodium homeostasis. It can be induced by exogenous sodium chloride and is one of the major kinases that regulates Na^+ intake by phosphorylation of epithelial sodium channels (ENaCs)[4, 5]. Considering the defects in Th17 development in *Sgk1*$^{-/-}$ mice, this raised the hypothesis that increasing sodium concentration may affect the Th17 cell phenotype through SGK1. To address this issue, we first activated naïve T cells in the presence of additional NaCl, but in the absence of any polarizing cytokines. Microarray analysis of these NaCl-treated cells showed a significant upregulation of *Sgk1* and of multiple other genes associated with Th17 development (Fisher exact test; $p<10^{-3}$**; Supplementary Table 2**; **Supplementary Fig. 7a**), which we confirmed by qPCR analysis of selected genes (**Supplementary Fig. 7b**). We also observed increased mRNA and protein levels of IL-17 and IL-23R with additional NaCl under various Th17 polarizing conditions (**Fig. 4a, b** and **Supplementary Fig. 7c**). Furthermore, a sodium-induced increase in Th17 development and IL-23R expression was not observed in SGK1-deficient T cells, specifically in the context of IL-23-IL-23R signaling (**Fig 4c, d**). Importantly, culturing cells with mannitol did not alter Th17 cell differentiation, excluding the possibility that the Th17 program is

initiated simply by the alteration of osmotic pressure (**Supplementary Fig. 7d**).

Recent studies have shown that different components in the daily diet and gut microbiota can strongly affect the frequency of effector T cells in the gut[14, 15]. Additionally, previous data indicates that molecules related to sodium homeostasis can influence Th17 cell responses[16, 17]. To further understand the effect of NaCl on Th17 cell generation *in vivo*, we fed a high salt diet (HSD) to WT or $Cd4^{Cre}Sgk1^{fl/fl}$ mice. After 3 weeks on HSD, we observed that unimmunized WT mice showed a marked increase in the frequency of Th17 cells in the lamina propria (LP), while no notable changes were observed in the mesenteric lymph nodes (mLN) or spleen. On the other hand, SGK1-deficient mice exhibited a much milder enhancement of Th17 cell frequency in the gut while there was no increase in IFN-γ production in any of the mice fed with HSD (**Supplementary Fig. 8a, b**).

Finally, we studied whether HSD would have an effect on the development of Th17 and EAE development *in vivo*. Mice fed HSD showed increased EAE severity when compared to the WT mice, which was dramatically reduced in SGK1-deficient mice **(Fig. 4e** and **Supplementary Fig. 8c,d)**. We also observed a significantly higher frequency of Th17 cells in mLN and CNS of WT mice fed with HSD, but not in SGK1-deficient mice. The percentage of IFN-γ producing T cells in the CNS, but not in the peripheral immune compartments, of WT mice was increased in mice fed HSD, suggesting that HSD may increase infiltration, but not expansion of IFN-γ^+ effector T cells, in the target organs (**Fig. 4f** and **Supplementary Fig. 8e**). Consistent with our *in vitro* data, we observed elevated

IL-17 but not IFN-γ, production from $CD4^+$ T cells isolated from EAE immunized WT mice fed with HSD and restimulated *in vitro* with MOG_{35-55} (**Supplementary Fig. 8f**). The data presented here indicates that high sodium intake potentiates Th17 cell generation *in vivo* in an SGK1-dependent manner and therefore has the potential to increase the risk of promoting autoimmunity.

In conclusion, we used a combination of microarray data analysis, large-scale protein-protein interaction network analysis and experimental data from multiple different knockout mice to establish IL-23R-SGK1-Foxo1 as a critical axis in Th17 stabilization. We show that Foxo1 acts as a repressor of IL-23R expression by directly binding to the *Il23r* promoter and inhibiting RORγt mediated *Il23r* transactivation. Phosphorylation of Foxo1, mediated by SGK1, leads to its deactivation and promotes unopposed RORγt-mediated *Il23r* transcription. SGK1 has been extensively studied in the context of NaCl transport[18, 19]. Modest increase of the NaCl concentration induces SGK1 expression in T cells with increased IL-23R expression and Th17 cell generation *in vitro*. Interestingly, even in unimmunized mice, enhancement of Th17 differentiation was observed *in vivo* in the gut and gut-associated lymphoid tissue and this increase in Th17 cells can be recalled at other peripheral sites following immunization. Although our data suggests an essential role for SGK1 in this process, it is likely that other immune cells and pathways are also influenced by increased salt intake. Furthermore, our result does not exclude additional alternative mechanisms by which an increase in NaCl affects Th17 cells. Nevertheless, the elevated *in vivo* Th17 differentiation by HSD raises the important issue of whether increased salt in the western diet and in processed foods is responsible

for an increased generation of pathogenic Th17 cells and for an unprecedented increase in autoimmune diseases in the western world.

Acknowledgements

We thank D. Kozoriz for cell sorting; Dr. Zhou. L, Dr. Accili. D, Dr. Demoulin. J and Dr. Sato K provide reagents. Supported by the US National Institutes of Health (NS030843, NS045937, AI073748 and AI045757 to V.K.K.; K01DK090105 to S.X. and the Austrian Science Fund (FWF, J 3091-B12). To T.T.

Authors' contribution

C.W, N.Y. and T.T. performed experiments and wrote the manuscript. C.Z., S.X. and Y.K. performed experiments. N.Y. analyzed the data. A.R. and V.K.K. supervised the study and edited the manuscript.

Author Information Reprints and permissions information is available at www.nature.com/reprints. The authors declare no competing financial interests. Readers are welcome to comment on the online version of the paper. Correspondence and requests for materials should be addressed to A.R. (aregev@broad.mit.edu) or V.K. (vkuchroo@rics.bwh.harvard.edu)

Methods Summary

Microarrays and network analysis. For gene expression analysis Affymetrix microarray chips were used. Data was processed using the GenePattern suite[20]. Differentially expressed genes were detected using fold-change and t-test analysis (for *Sgk1*$^{-/-}$ and NaCl-treated T cells), a consensus of fold-change, the EDGE software[21] and a novel sigmoid-based method[22] (for the *Il23r*$^{-/-}$ Th17 cell time course data). A command-line version of the ANAT software[9] was used for network analysis.

***In vitro* T cell differentiation.** Naïve T cells were FACS-sorted, stimulated with plate bound anti-CD3/CD28 and the indicated cytokines or NaCl and cells were analyzed by qPCR or flow cytometry at different time points.

EAE model. Mice were immunized subcutaneously with MOG_{35-55}, CFA, heat-inactivated *Mycobacterium tuberculosis* and with intraperitoneal injection of *Bordatella pertussis* toxin.

***In vivo* cell transfer.** Naïve T cells were differentiated towards Th17 cells, then transferred into MOG_{35-55}/CFA immunized hosts and T cells isolated from various organs were analyzed by flow cytometry at 7-12 days after onset of EAE.

Western Blot/Immunoprecipitation. Differentiated T cells or transfected HEK293T cells were lysed in WCE buffer and lysates were subjected to Western blot or immunoprecipitation analysis.

Promoter activity reporter assay. HEK 293T cells were transfected with luciferase reporter constructs and expression vectors and luciferase expression was determined after 48 h.

Reference:

1. Korn T, Bettelli E, Oukka M, Kuchroo VK. IL-17 and Th17 Cells. *Annu Rev Immunol* 2009, **27:** 485-517.

2. Aggarwal S, Ghilardi N, Xie MH, de Sauvage FJ, Gurney AL. Interleukin-23 promotes a distinct CD4 T cell activation state characterized by the production of interleukin-17. *J Biol Chem* 2003, **278**(3)**:** 1910-1914.

3. Zhou L, Ivanov, II, Spolski R, Min R, Shenderov K, Egawa T, *et al.* IL-6 programs T(H)-17 cell differentiation by promoting sequential engagement of the IL-21 and IL-23 pathways. *Nat Immunol* 2007, **8**(9)**:** 967-974.

4. Lang F, Bohmer C, Palmada M, Seebohm G, Strutz-Seebohm N, Vallon V. (Patho)physiological significance of the serum- and glucocorticoid-inducible kinase isoforms. *Physiol Rev* 2006, **86**(4)**:** 1151-1178.

5. Wulff P, Vallon V, Huang DY, Volkl H, Yu F, Richter K, *et al.* Impaired renal Na(+) retention in the sgk1-knockout mouse. *The Journal of clinical investigation* 2002, **110**(9)**:** 1263-1268.

6. Salker MS, Christian M, Steel JH, Nautiyal J, Lavery S, Trew G, *et al.* Deregulation of the serum- and glucocorticoid-inducible kinase SGK1 in the endometrium causes reproductive failure. *Nature medicine* 2011, **17**(11)**:** 1509-1513.

7. Zhang L, Cui R, Cheng X, Du J. Antiapoptotic effect of serum and glucocorticoid-inducible protein kinase is mediated by novel mechanism activating I{kappa}B kinase. *Cancer Res* 2005, **65**(2)**:** 457-464.

8. Shelly C, Herrera R. Activation of SGK1 by HGF, Rac1 and integrin-mediated cell adhesion in MDCK cells: PI-3K-dependent and -independent pathways. *J Cell Sci* 2002, **115**(Pt 9)**:** 1985-1993.

9. Yosef N, Zalckvar E, Rubinstein AD, Homilius M, Atias N, Vardi L, *et al.* ANAT: a tool for constructing and analyzing functional protein networks. *Sci Signal* 2011, **4**(196)**:** pl1.

10. Brunet A, Park J, Tran H, Hu LS, Hemmings BA, Greenberg ME. Protein kinase SGK mediates survival signals by phosphorylating the forkhead transcription factor FKHRL1 (FOXO3a). *Mol Cell Biol* 2001, **21**(3)**:** 952-965.

11. Wei G, Wei L, Zhu J, Zang C, Hu-Li J, Yao Z, *et al.* Global mapping of H3K4me3 and H3K27me3 reveals specificity and plasticity in lineage fate determination of differentiating CD4+ T cells. *Immunity* 2009, **30**(1)**:** 155-167.

12. Di Pietro N, Panel V, Hayes S, Bagattin A, Meruvu S, Pandolfi A, *et al.* Serum- and glucocorticoid-inducible kinase 1 (SGK1) regulates adipocyte differentiation via forkhead box O1. *Mol Endocrinol* 2010, **24**(2)**:** 370-380.

13. Essaghir A, Dif N, Marbehant CY, Coffer PJ, Demoulin JB. The transcription of FOXO genes is stimulated by FOXO3 and repressed by growth factors. *J Biol Chem* 2009, **284**(16)**:** 10334-10342.

14. Berer K, Mues M, Koutrolos M, Rasbi ZA, Boziki M, Johner C, *et al.* Commensal microbiota and myelin autoantigen cooperate to trigger autoimmune demyelination. *Nature* 2011, **479**(7374)**:** 538-541.

15. Sczesnak A, Segata N, Qin X, Gevers D, Petrosino JF, Huttenhower C, *et al.* The genome of th17 cell-inducing segmented filamentous bacteria reveals extensive auxotrophy and adaptations to the intestinal environment. *Cell Host Microbe* 2011, **10**(3)**:** 260-272.

16. Stegbauer J, Lee DH, Seubert S, Ellrichmann G, Manzel A, Kvakan H, *et al.* Role of the renin-angiotensin system in autoimmune inflammation of the central nervous system. *Proceedings of the National Academy of Sciences of the United States of America* 2009, **106**(35)**:** 14942-14947.

17. Herrada AA, Contreras FJ, Marini NP, Amador CA, Gonzalez PA, Cortes CM, *et al.* Aldosterone promotes autoimmune damage by enhancing Th17-mediated immunity. *J Immunol* 2010, **184**(1)**:** 191-202.

18. Diakov A, Korbmacher C. A novel pathway of epithelial sodium channel activation involves a serum- and glucocorticoid-inducible kinase consensus motif in the C terminus of the channel's alpha-subunit. *J Biol Chem* 2004, **279**(37)**:** 38134-38142.

19. Loffing J, Zecevic M, Feraille E, Kaissling B, Asher C, Rossier BC, *et al.* Aldosterone induces rapid apical translocation of ENaC in early portion of renal collecting system: possible role of SGK. *Am J Physiol Renal Physiol* 2001, **280**(4)**:** F675-682.

20. Reich M, Liefeld T, Gould J, Lerner J, Tamayo P, Mesirov JP. GenePattern 2.0. *Nat Genet* 2006, **38**(5)**:** 500-501.

21. Storey JD, Xiao W, Leek JT, Tompkins RG, Davis RW. Significance analysis of time course microarray experiments. *Proceedings of the National Academy of Sciences of the United States of America* 2005, **102**(36)**:** 12837-12842.

22. Chechik G, Koller D. Timing of gene expression responses to environmental changes. *J Comput Biol* 2009, **16**(2)**:** 279-290.

Fig 1

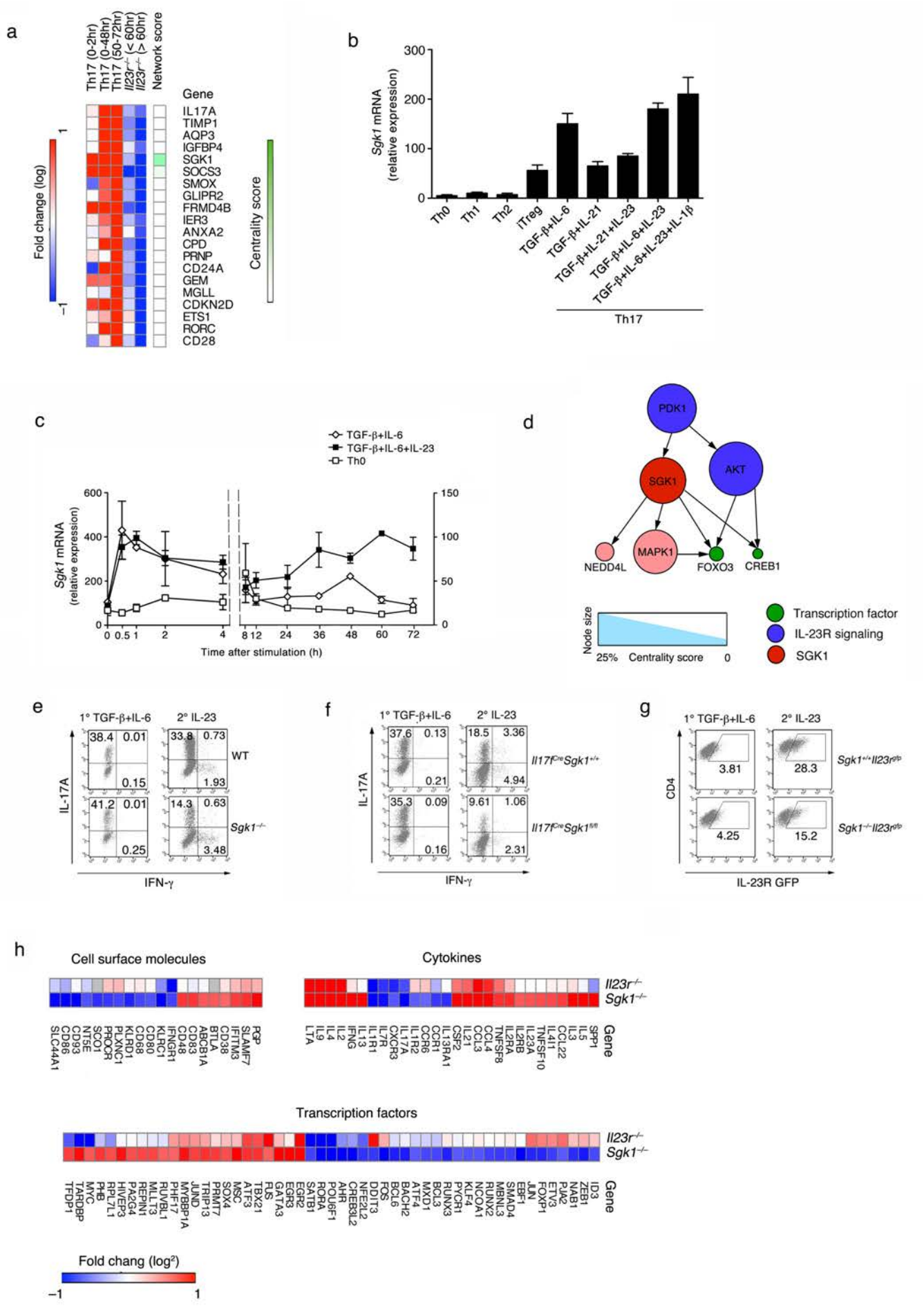
a
Th17 (0-2hr)
Th17 (0-48hr)
Th17 (50-72hr)
Il23r−/− (< 60hr)
Il23r−/− (> 60hr)
Network score
Gene
IL17A
TIMP1
AQP3
IGFBP4
SGK1
SOCS3
SMOX
GLIPR2
FRMD4B
IER3
ANXA2
CPD
PRNP
CD24A
GEM
MGLL
CDKN2D
ETS1
RORC
CD28
Fold change (log)
1
−1
Centrality score
b
Sgk1 mRNA (relative expression)
300
200
100
0
Th0
Th1
Th2
iTreg
TGF-β+IL-6
TGF-β+IL-21
TGF-β+IL-21+IL-23
TGF-β+IL-6+IL-23
TGF-β+IL-6+IL-23+IL-1β
Th17
c
TGF-β+IL-6
TGF-β+IL-6+IL-23
Th0
Sgk1 mRNA (relative expression)
600
400
200
0
150
100
50
0
0 0.5 1 2 4 8 12 24 36 48 60 72
Time after stimulation (h)
d
PDK1
SGK1
AKT
NEDD4L
MAPK1
FOXO3
CREB1
Node size
25%
Centrality score
0
Transcription factor
IL-23R signaling
SGK1
e
1° TGF-β+IL-6
2° IL-23
38.4
0.01
0.15
33.8
0.73
1.93
WT
41.2
0.01
0.25
14.3
0.63
3.48
Sgk1−/−
IL-17A
IFN-γ
f
1° TGF-β+IL-6
2° IL-23
37.6
0.13
0.21
18.5
3.36
4.94
Il17fCreSgk1+/+
35.3
0.09
0.16
9.61
1.06
2.31
Il17fCreSgk1fl/fl
IL-17A
IFN-γ
g
1° TGF-β+IL-6
2° IL-23
3.81
28.3
Sgk1+/+Il23rgfp
4.25
15.2
Sgk1−/−Il23rgfp
CD4
IL-23R GFP
h
Cell surface molecules
Cytokines
Il23r−/−
Sgk1−/−
SLC44A1 CD86 CD93 NT5E SCO1 PROCR PLXNC1 KLRD1 CD68 CD80 KLRC1 IFNGR1 CD48 CD83 ABCB1A BTLA CD38 IFITM3 SLAMF7 PGP
IL17A IL7R CXCR3 IL1R2 CCR6 CCR1 IL13RA1 CSF2 IL21 CCL3 CCL4 TNFSF8 IL2RA IL2RB IL23A TNFSF10 IL4I1 CCL22 IL3 IL5 SPP1
Gene
Transcription factors
Il23r−/−
Sgk1−/−
TFDP1 TARDBP MYC PHB HIVEP3 RPL7L1 PA2G4 REPIN1 MLLT3 RUVBL1 PHF17 MYBBP1A JUND TRIP13 PRMT7 SOX4 MSC ATF3 TBX21 FUS GATA3 EGR3 EGR2 SATB1 IL9 RORA POU6F1 AHR CREB3L2 NFE2L2 DDIT3 FOS BCL6 BACH2 ATF4 MXD1 BCL3 RUNX3 PYCR1 KLF4 NCOA1 RUNX2 MBNL3 SMAD4 EBF1 JUN FOXP1 ETV3 PJA2 NAB1 ZEB1 ID3
Gene
Fold chang (log2)
−1
1

Fig 2

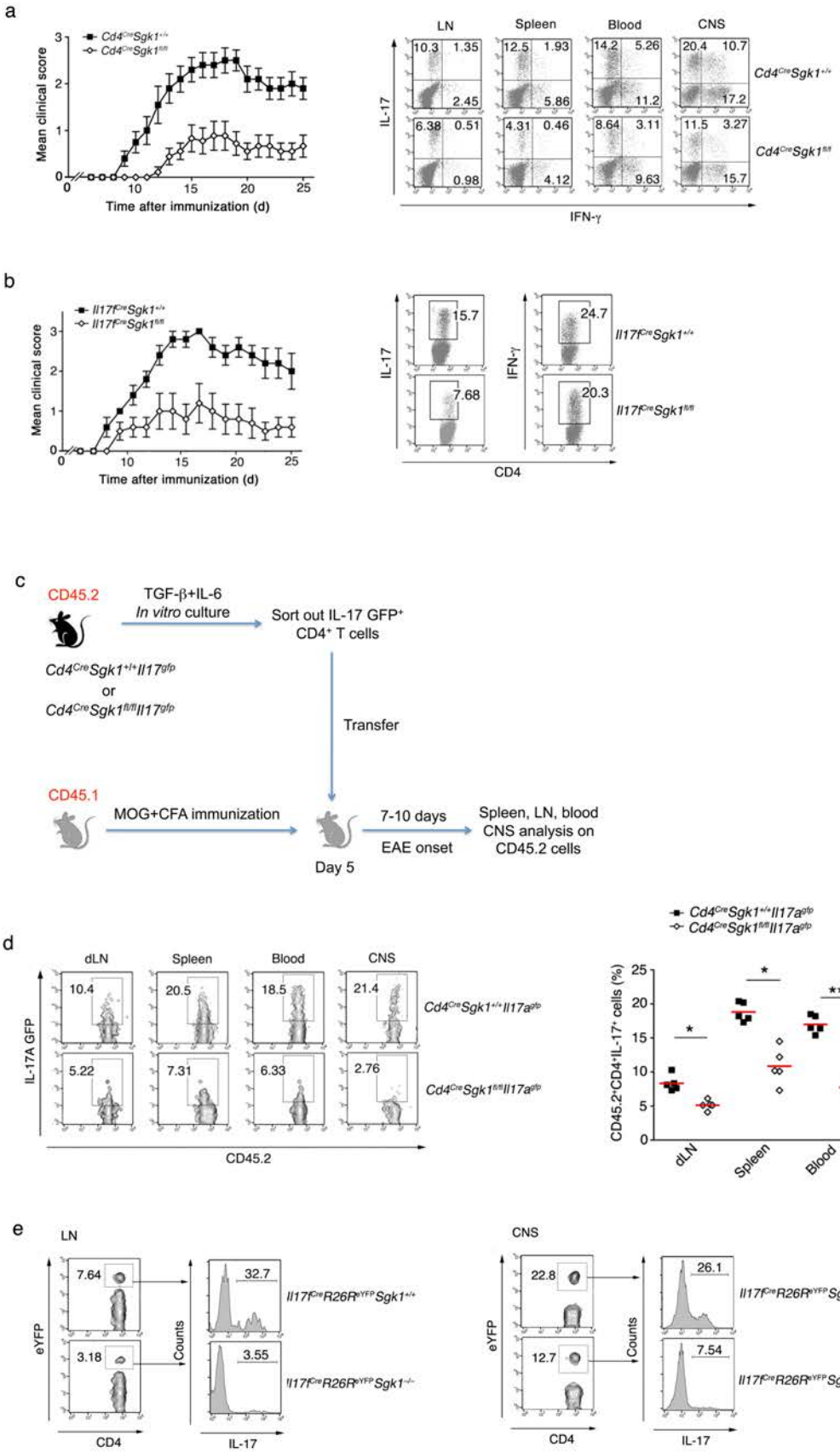
a
Mean clinical score
Time after immunization (d)
LN
Spleen
Blood
CNS
IL-17
IFN-γ
b
Mean clinical score
Time after immunization (d)
IL-17
IFN-γ
CD4
c
CD45.2
TGF-β+IL-6
In vitro culture
Sort out IL-17 GFP+ CD4+ T cells
or
Transfer
CD45.1
MOG+CFA immunization
7-10 days
EAE onset
Spleen, LN, blood CNS analysis on CD45.2 cells
Day 5
d
dLN
Spleen
Blood
CNS
IL-17A GFP
CD45.2
CD45.2+CD4+IL-17+ cells (%)
e
LN
CNS
eYFP
Counts
CD4
IL-17

Fig 3

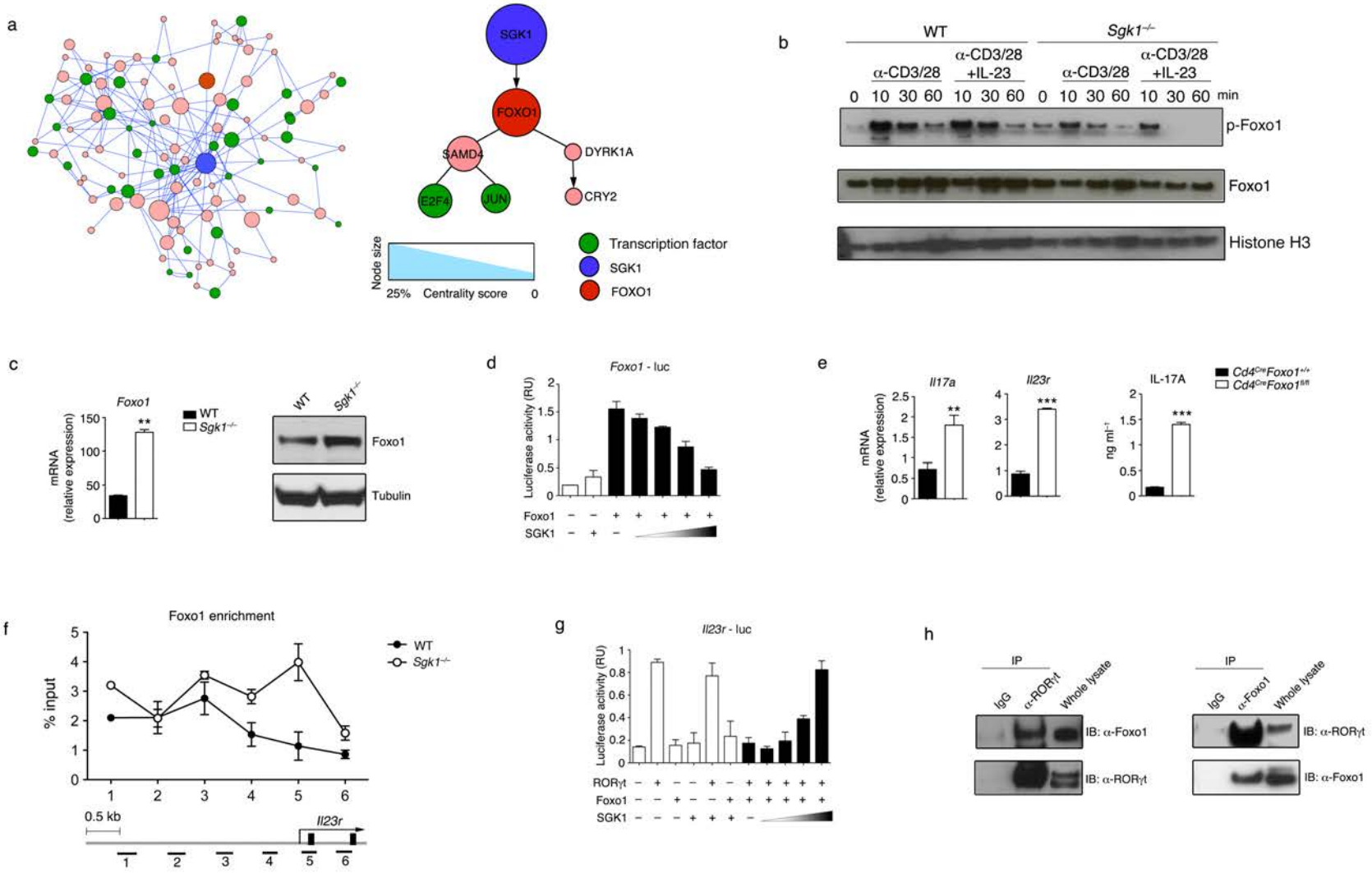
a
SGK1
FOXO1
SAMD4
DYRK1A
E2F4
JUN
CRY2
Node size
25%
Centrality score
0
Transcription factor
SGK1
FOXO1
b
WT
Sgk1−/−
α-CD3/28
α-CD3/28 +IL-23
0 10 30 60 10 30 60 0 10 30 60 10 30 60 min
p-Foxo1
Foxo1
Histone H3
c
Foxo1
mRNA (relative expression)
WT
Sgk1−/−
Tubulin
d
Foxo1 - luc
Luciferase acitivity (RU)
Foxo1
SGK1
e
Il17a
Il23r
IL-17A
mRNA (relative expression)
ng ml−1
Cd4Cre Foxo1+/+
Cd4Cre Foxo1fl/fl
f
Foxo1 enrichment
% input
0.5 kb
Il23r
g
Il23r - luc
Luciferase acitivity (RU)
RORγt
Foxo1
SGK1
h
IP
IgG
α-RORγt
Whole lysate
IB: α-Foxo1
IB: α-RORγt
α-Foxo1

Fig 4

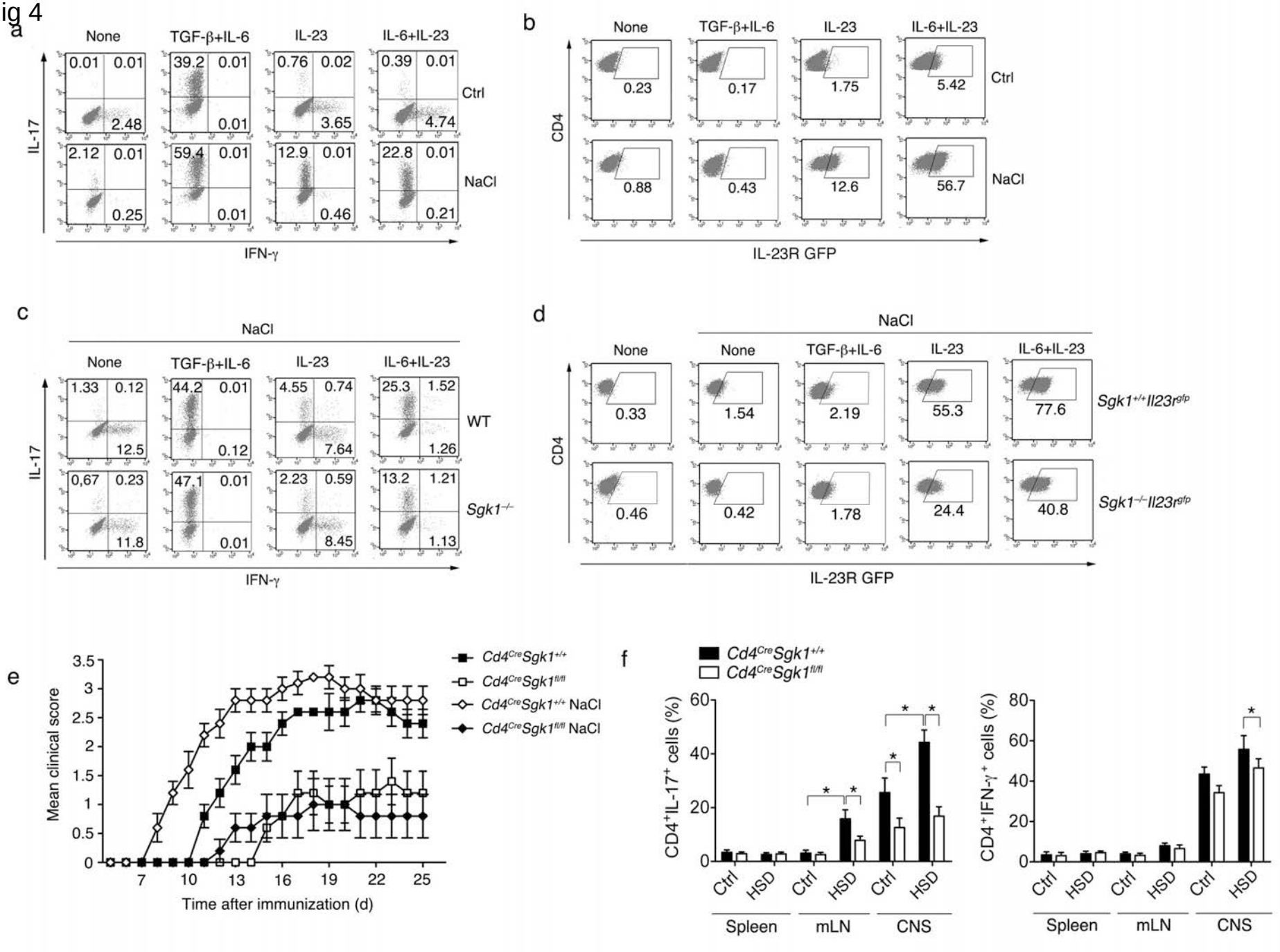
a
None
TGF-β+IL-6
IL-23
IL-6+IL-23
Ctrl
NaCl
IL-17
IFN-γ
0.01 0.01 2.48 0.25
39.2 0.01 0.01 0.01
0.76 0.02 3.65 0.46
0.39 0.01 4.74 0.21
2.12 0.01 0.25
59.4 0.01 0.01
12.9 0.01 0.46
22.8 0.01 0.21
b
None
TGF-β+IL-6
IL-23
IL-6+IL-23
Ctrl
NaCl
CD4
IL-23R GFP
0.23
0.17
1.75
5.42
0.88
0.43
12.6
56.7
c
NaCl
None
TGF-β+IL-6
IL-23
IL-6+IL-23
WT
Sgk1−/−
IL-17
IFN-γ
1.33 0.12 12.5
44.2 0.01 0.12
4.55 0.74 7.64
25.3 1.52 1.26
0,67 0.23 11.8
47.1 0.01 0.01
2.23 0.59 8.45
13.2 1.21 1.13
d
NaCl
None
None
TGF-β+IL-6
IL-23
IL-6+IL-23
Sgk1+/+Il23rgfp
Sgk1−/−Il23rgfp
CD4
IL-23R GFP
0.33
1.54
2.19
55.3
77.6
0.46
0.42
1.78
24.4
40.8
e
Cd4CreSgk1+/+
Cd4CreSgk1fl/fl
Cd4CreSgk1+/+ NaCl
Cd4CreSgk1fl/fl NaCl
Mean clinical score
Time after immunization (d)
f
Cd4CreSgk1+/+
Cd4CreSgk1fl/fl
CD4+IL-17+ cells (%)
CD4+IFN-γ+ cells (%)
Ctrl
HSD
Spleen
mLN
CNS

Sup Fig 1

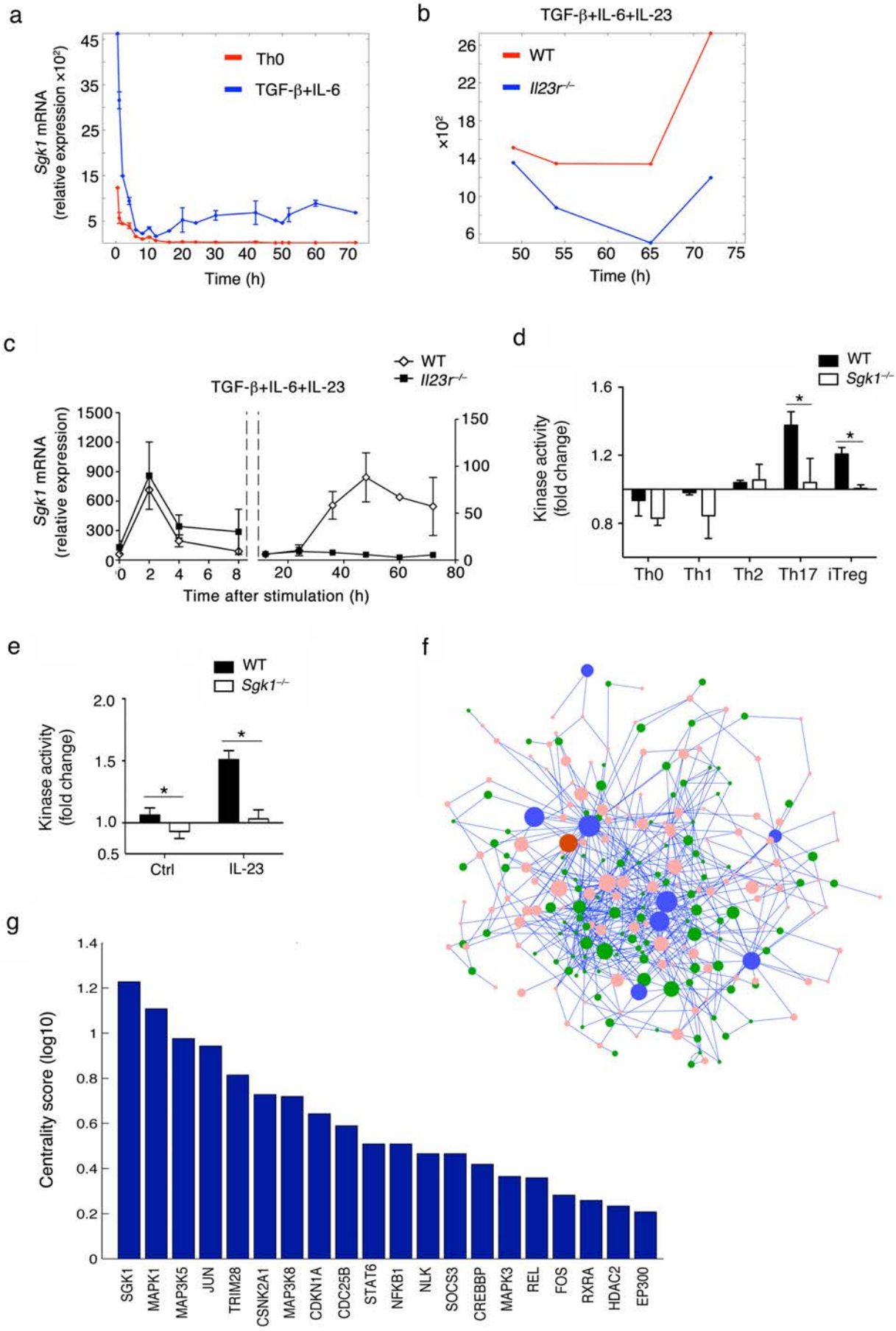
a
Sgk1 mRNA (relative expression ×10²)
Th0
TGF-β+IL-6
Time (h)
b
TGF-β+IL-6+IL-23
WT
Il23r−/−
×10²
Time (h)
c
TGF-β+IL-6+IL-23
WT
Il23r−/−
Sgk1 mRNA (relative expression)
Time after stimulation (h)
d
WT
Sgk1−/−
Kinase activity (fold change)
Th0
Th1
Th2
Th17
iTreg
e
WT
Sgk1−/−
Kinase activity (fold change)
Ctrl
IL-23
f
g
Centrality score (log10)
SGK1
MAPK1
MAP3K5
JUN
TRIM28
CSNK2A1
MAP3K8
CDKN1A
CDC25B
STAT6
NFKB1
NLK
SOCS3
CREBBP
MAPK3
REL
FOS
RXRA
HDAC2
EP300

Sup Fig 2

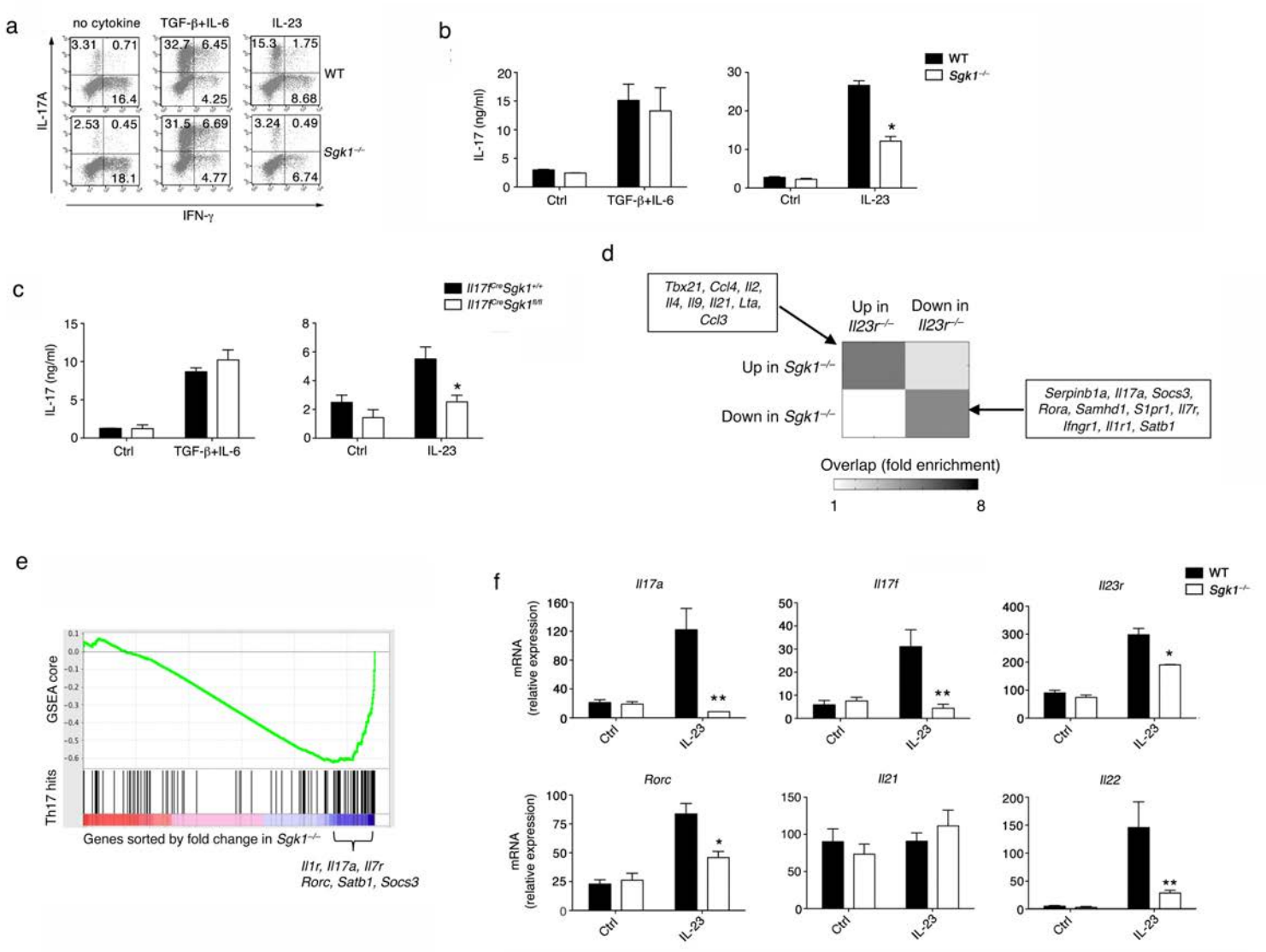
a
no cytokine
TGF-β+IL-6
IL-23
IL-17A
IFN-γ
WT
Sgk1−/−
3.31
0.71
16.4
32.7
6.45
4.25
15.3
1.75
8.68
2.53
0.45
18.1
31.5
6.69
4.77
3.24
0.49
6.74
b
IL-17 (ng/ml)
Ctrl
TGF-β+IL-6
IL-23
WT
Sgk1−/−
c
Il17fCreSgk1+/+
Il17fCreSgk1fl/fl
IL-17 (ng/ml)
Ctrl
TGF-β+IL-6
IL-23
d
Tbx21, Ccl4, Il2, Il4, Il9, Il21, Lta, Ccl3
Up in Il23r−/−
Down in Il23r−/−
Up in Sgk1−/−
Down in Sgk1−/−
Serpinb1a, Il17a, Socs3, Rora, Samhd1, S1pr1, Il7r, Ifngr1, Il1r1, Satb1
Overlap (fold enrichment)
1
8
e
GSEA core
Th17 hits
Genes sorted by fold change in Sgk1−/−
Il1r, Il17a, Il7r
Rorc, Satb1, Socs3
f
Il17a
Il17f
Il23r
Rorc
Il21
Il22
mRNA (relative expression)
Ctrl
IL-23
WT
Sgk1−/−

Sup Fig 3

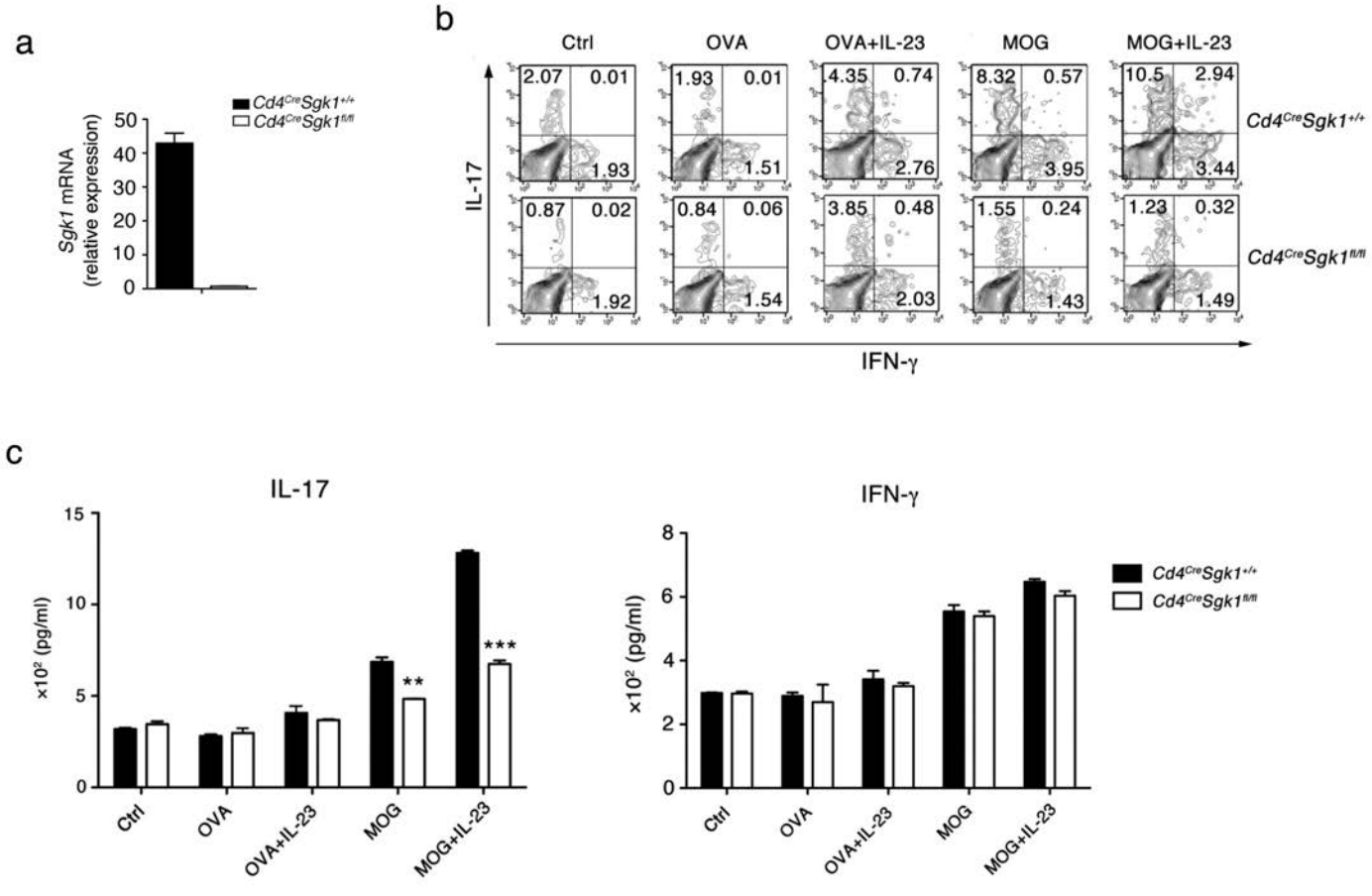
a
Cd4CreSgk1+/+
Cd4CreSgk1fl/fl
Sgk1 mRNA (relative expression)
50
40
30
20
10
0
b
Ctrl
OVA
OVA+IL-23
MOG
MOG+IL-23
IL-17
IFN-γ
2.07
0.01
1.93
1.51
4.35
0.74
2.76
8.32
0.57
3.95
10.5
2.94
3.44
0.87
0.02
1.92
0.84
0.06
1.54
3.85
0.48
2.03
1.55
0.24
1.43
1.23
0.32
1.49
Cd4CreSgk1+/+
Cd4CreSgk1fl/fl
c
IL-17
IFN-γ
×10² (pg/ml)
15
10
5
0
8
6
4
2
0
**
***
Ctrl
OVA
OVA+IL-23
MOG
MOG+IL-23
Cd4CreSgk1+/+
Cd4CreSgk1fl/fl

Sup Fig 4

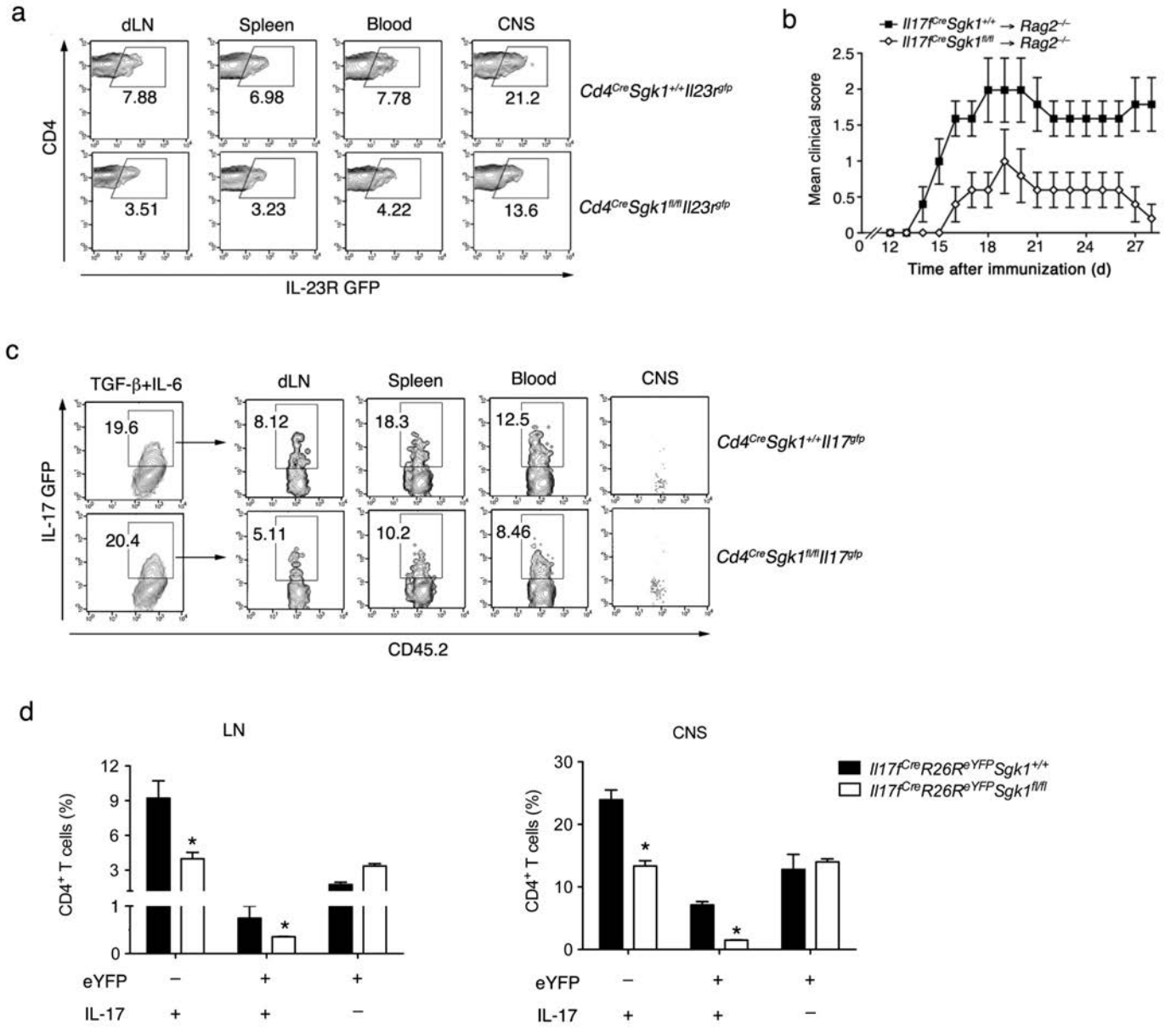
a
dLN
Spleen
Blood
CNS
CD4
7.88
6.98
7.78
21.2
3.51
3.23
4.22
13.6
Cd4CreSgk1+/+Il23rgfp
Cd4CreSgk1fl/flIl23rgfp
IL-23R GFP
b
Il17fCreSgk1+/+ → Rag2−/−
Il17fCreSgk1fl/fl → Rag2−/−
Mean clinical score
Time after immunization (d)
c
TGF-β+IL-6
dLN
Spleen
Blood
CNS
IL-17 GFP
19.6
20.4
8.12
5.11
18.3
10.2
12.5
8.46
Cd4CreSgk1+/+Il17gfp
Cd4CreSgk1fl/flIl17gfp
CD45.2
d
LN
CNS
CD4+ T cells (%)
Il17fCreR26ReYFPSgk1+/+
Il17fCreR26ReYFPSgk1fl/fl
eYFP
IL-17

Sup Fig 5

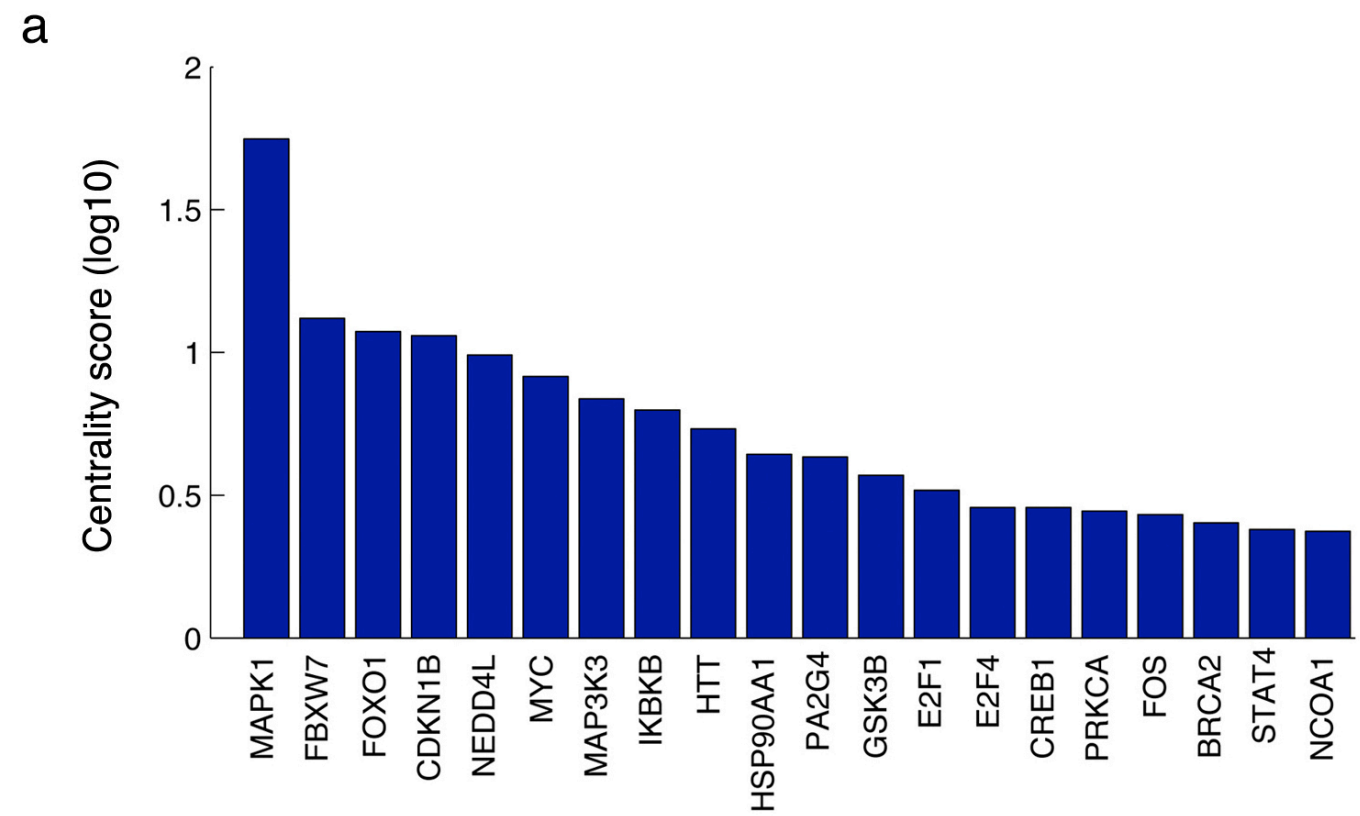
a
Centrality score (log10)
2
1.5
1
0.5
0
MAPK1
FBXW7
FOXO1
CDKN1B
NEDD4L
MYC
MAP3K3
IKBKB
HTT
HSP90AA1
PA2G4
GSK3B
E2F1
E2F4
CREB1
PRKCA
FOS
BRCA2
STAT4
NCOA1

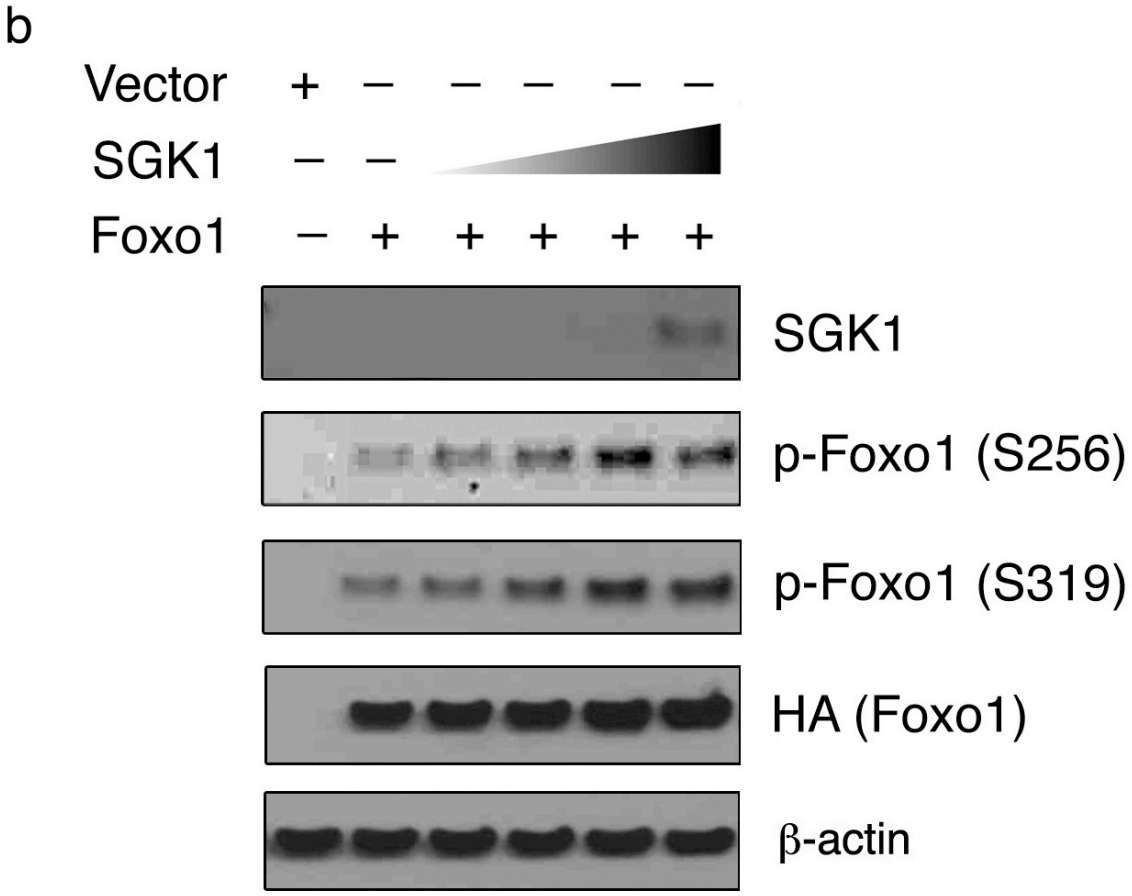
b
Vector + – – – – –
SGK1 – –
Foxo1 – + + + + +
SGK1
p-Foxo1 (S256)
p-Foxo1 (S319)
HA (Foxo1)
β-actin

Sup Fig 6

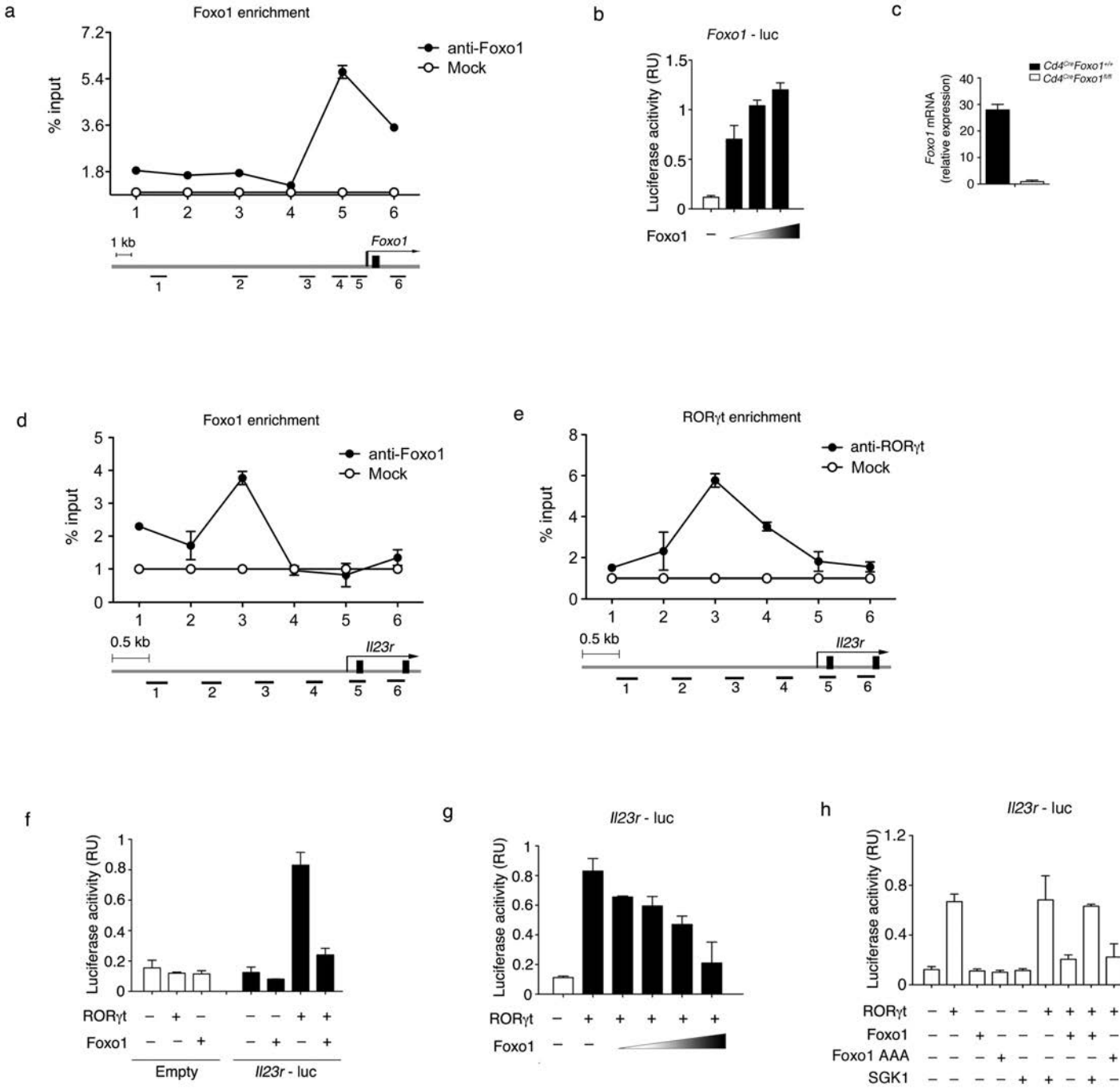
a
Foxo1 enrichment
% input
anti-Foxo1
Mock
1 kb
Foxo1
b
Foxo1 - luc
Luciferase acitivity (RU)
Foxo1
c
Cd4Cre Foxo1+/+
Cd4Cre Foxo1fl/fl
Foxo1 mRNA (relative expression)
d
Foxo1 enrichment
anti-Foxo1
Mock
0.5 kb
Il23r
e
RORγt enrichment
anti-RORγt
Mock
f
RORγt
Foxo1
Empty
Il23r - luc
g
Il23r - luc
h
Il23r - luc
RORγt
Foxo1
Foxo1 AAA
SGK1

Sup Fig 7

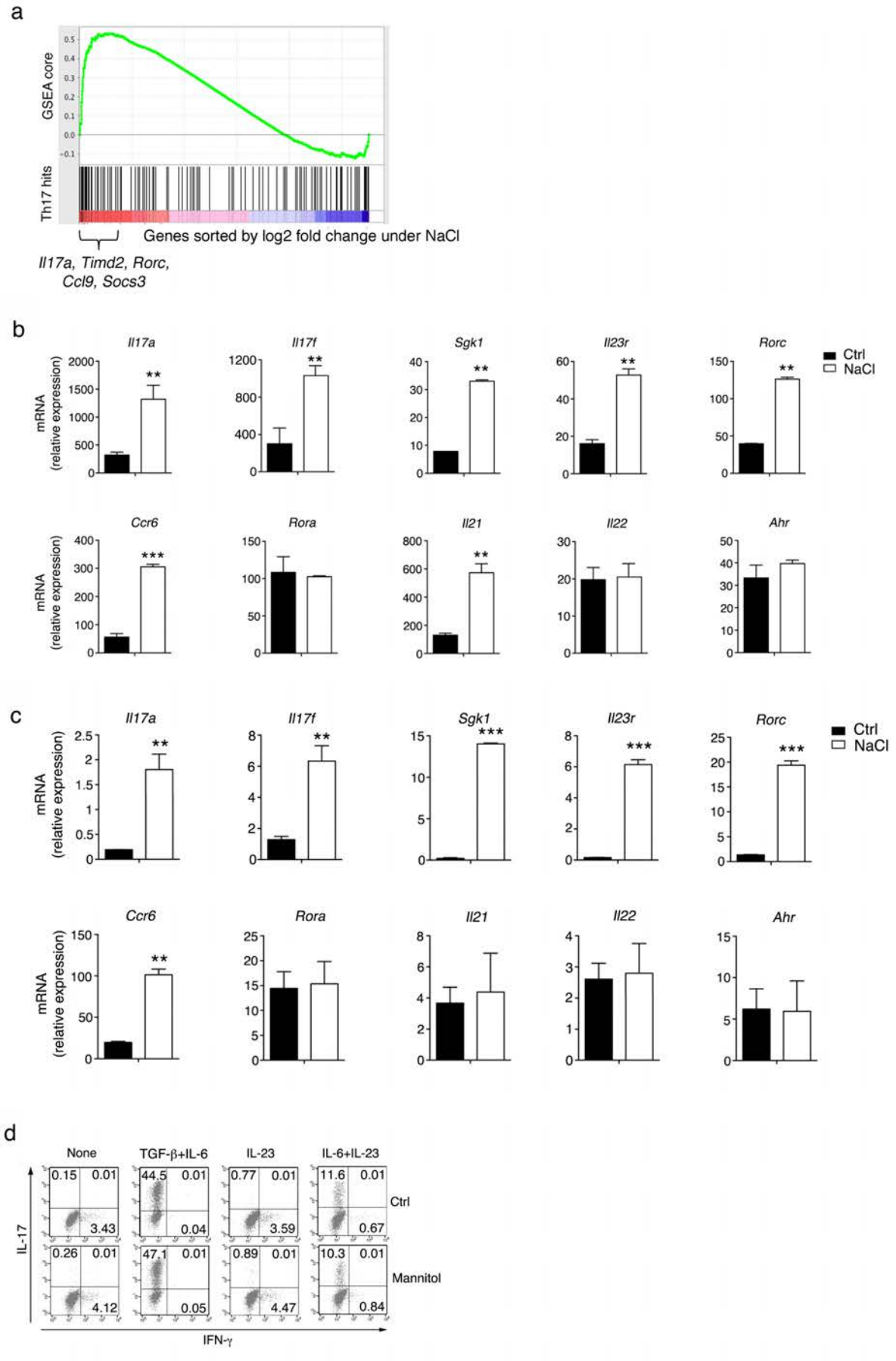
a
GSEA core
Th17 hits
Genes sorted by log2 fold change under NaCl
Il17a, Timd2, Rorc, Ccl9, Socs3
b
Il17a
Il17f
Sgk1
Il23r
Rorc
Ccr6
Rora
Il21
Il22
Ahr
mRNA (relative expression)
Ctrl
NaCl
c
d
None
TGF-β+IL-6
IL-23
IL-6+IL-23
Ctrl
Mannitol
IL-17
IFN-γ

Sup Fig 8

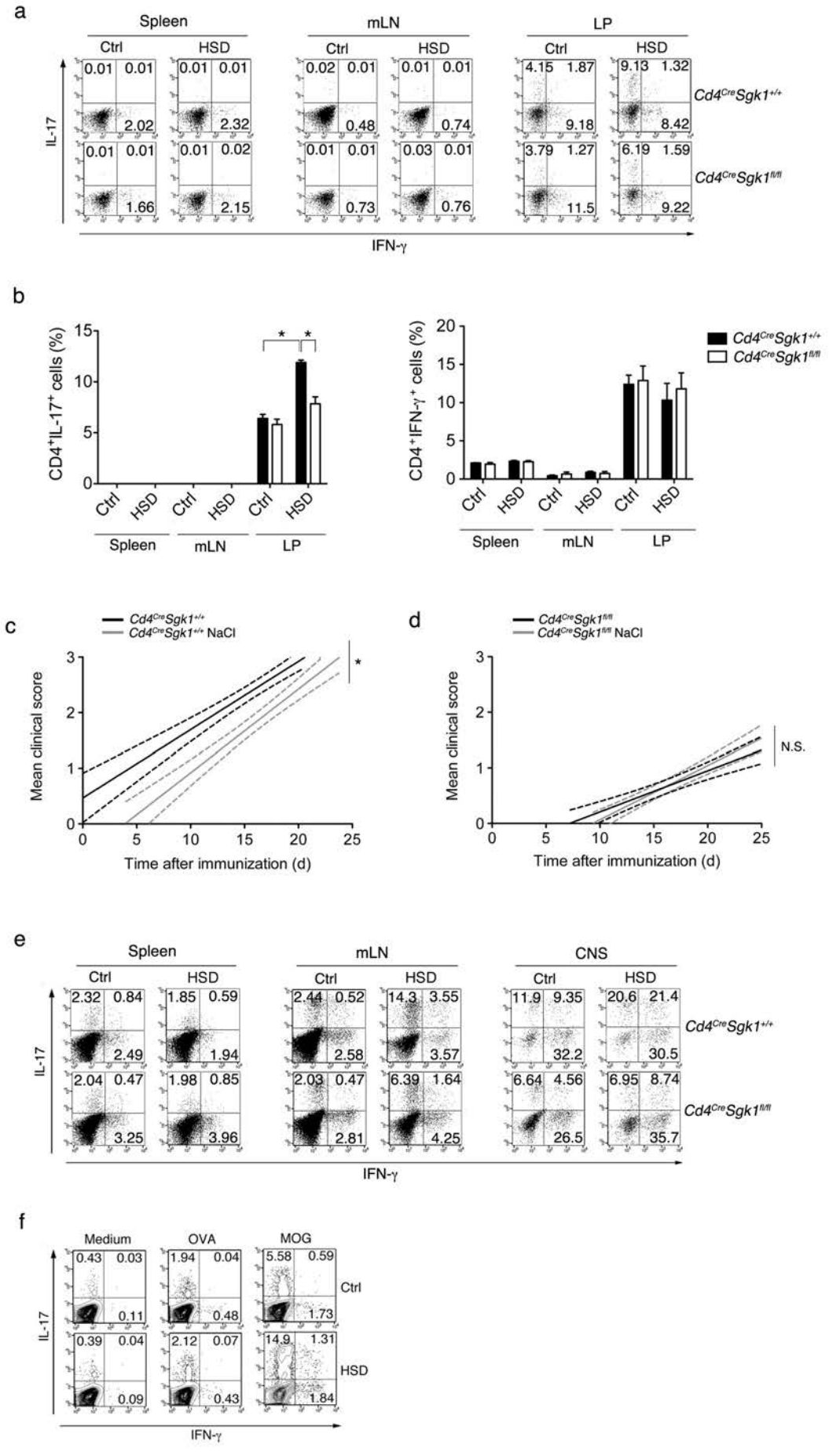
a
Spleen
mLN
LP
Ctrl
HSD
IL-17
IFN-γ
Cd4CreSgk1+/+
Cd4CreSgk1fl/fl
b
CD4+IL-17+ cells (%)
CD4+IFN-γ+ cells (%)
Spleen
mLN
LP
c
Cd4CreSgk1+/+
Cd4CreSgk1+/+ NaCl
Mean clinical score
Time after immunization (d)
d
Cd4CreSgk1fl/fl
Cd4CreSgk1fl/fl NaCl
N.S.
e
CNS
f
Medium
OVA
MOG

Figure legends

Figure 1. SGK1 is specifically induced in Th17 cells and is important for their maintenance. (a) Top candidate genes ranked by their average of fold-increase in Th17 conditions (TGF-β1 with IL-6 compared to Th0) and fold decrease in *Il23r*$^{-/-}$ (KO vs. WT cells, TGF-β1, IL-6 and IL-23 condition). The network score of a given protein is the percentage of IL23-R-affected transcription factors downstream of that protein in the network (Methods); (b) SGK1 mRNA expression in different T cell subsets; (c) Kinetic analysis of SGK1 gene expression in activated naïve WT CD4^{+} T cells differentiated with TGF-β, IL-6 and IL-23; (d) IL-23R protein-protein interaction network model. Zooming in on the SGK1 sub-network in Supplementary Fig. 1f. Nodes are sized proportionally to their network score; (e-g) Naïve CD4^{+} T cells from *Sgk1*$^{-/-}$ (e), *Il17f*^{Cre}*Sgk1*$^{fl/fl}$ (f) or *Sgk1*$^{-/-}$*Il23r*^{gfp} (g) and control mice were differentiated into Th17 cells with TGF-β1 and IL-6 (left) or restimulated with IL-23 (right). IL-17 and IFN-γ or IL-23R (GFP) expression were assessed; (h) Heat map displaying microarray data, fold change of selected gene subsets in the two experimental settings: *Sgk1*$^{-/-}$ vs. WT, and *Il23r*$^{-/-}$ vs. WT Th17 cells (TGF-β1 and IL-6, restimulated with IL-23). Only genes with a significant fold change in the *Sgk1*$^{-/-}$ Th17 cells are presented. Data are representative of three independent experiments (error bars, SD)

Figure 2. SGK1 deficient mice are resistant to EAE due to defect in maintaining Th17 phenotype. (a) EAE development in *Cd4*^{Cre}*Sgk1*$^{+/+}$ and *Cd4*^{Cre}*Sgk1*$^{fl/fl}$ mice (left) and IL-17 and IFN-γ secretion by CD4^{+} T cells isolated from indicated organs at the peak

of disease (right) (n=12); (b) EAE development in *Il17f*^{Cre}*Sgk1*$^{+/+}$ and *Il17f*^{Cre}*Sgk1*$^{fl/fl}$ mice (left) and IL-17 and IFN-γ secretion by CD4^{+} T cells within the CNS (right) (n=10); (c) Schematic illustration of adoptive transfer experiments shown in (d); (d) IL-17 production from the donor CD4^{+} cells harvested from the indicated organs 12 days after transfer; representative histograms (left) and quantification of the FLOW CYTOMETRY data (right) (n=10); (e) IL-17A production by CD4^{+}eYFP^{+} T cells isolated from LN or CNS of WT and SGK1-deficient *Il17f*^{Cre}*R26R*^{eYFP} fate-reporter mice 17 days after MOG/CFA immunization. (n=10) **P*< 0.05, ***P*< 0.01 and ****P*< 0.001 (Student's *t*-test, error bars, SD).

Figure 3. SGK1 signaling promotes IL-23R expression through phosphorylation of Foxo1. (a) SGK1 protein-protein interaction network model. Left, network composed of all the protein nodes with a p-value under 10^{-4} (Methods); Right, zooming in on the Foxo1 sub-network. Nodes are sized proportional to their network score. Directed edges correspond to post-translational modifications. Non-directed edges correspond to protein-protein interactions with no known directionality; (b) Phosphorylated (pS256) and total Foxo1 levels were assessed in nuclear extracts after re-stimulation of WT and *Sgk1*$^{-/-}$ Th17 cells; (c) mRNA (left) and protein (right) levels of Foxo1 were analyzed 3 days after IL-23 restimulation of differentiated Th17 cells; (d) HEK293T cells were transfected with a *Foxo1* promoter-driven luciferase reporter along with the indicated plasmids and promoter activity was assessed; (e) Memory CD4^{+} T cells from *Foxo1*$^{-/-}$ mice were stimulated for 24 h with PMA and ionomycin and IL-17A and IL-23R expression was determined by qPCR or ELISA (IL-17A); (f) The binding of Foxo1 to the

Il23r promoter in WT and *Sgk1*$^{-/-}$ IL-23-restimulated Th17 cells was assayed by ChIP-PCR; (g) *Il23r* promoter activity was measured in HEK293T cells transfected with an *Il23r* promoter-driven luciferase reporter along with the indicated plasmids; (h) Immunoprecipitation (control IgG, anti-RORγt or anti-Foxo1) of lysates of WT IL-23 restimulated Th17 cells, followed by immunoblot analysis with indicated antibodies. ***P*< 0.01 and ****P*< 0.001 (Student's *t*-test). Data are representative of three independent experiments (error bars, SD).

Figure 4. NaCl potentiates Th17 cell differentiation *in vitro* and *in* vivo, enhancing EAE induction. (a) IL-17 and IFN-γ production by naïve WT CD4$^+$ T cells stimulated with indicated cytokines for 3 days +/− additional 40 mM NaCl; (b) IL-23R (GFP) expression in *Il23r*^{gfp} CD4$^+$ T cells stimulated under conditions described in (a); (c) IL-17 and IFN-γ production by WT and *Sgk1*$^{-/-}$ CD4$^+$ T cells stimulated with the indicated cytokines in the presence of 40 mM NaCl; (d) IL-23R (GFP) expression in *Sgk1*$^{-/-}$ *Il23r*^{gfp}and control CD4$^+$ T cells stimulated under conditions described in (c); (e) Clinical scores of EAE in *Cd4*^{Cre}*Sgk1*$^{+/+}$ and *Cd4*^{Cre}*Sgk1*$^{fl/fl}$ mice fed with high salt diet (HSD) or control diet (n=15); (f) Quantification of CD4$^+$IL-17$^+$ or CD4$^+$IFN-γ$^+$ T cells from the indicated organs of *Cd4*^{Cre}*Sgk1*$^{+/+}$ and *Cd4*^{Cre}*Sgk1*$^{fl/fl}$ mice fed HSD or control diet; on day 17 following immunization with MOG/CFA. **P*< 0.05 (Student's *t*-test). Data are representative of three independent experiments (error bars, SD).

Supplementary Information

Supplementary Fig. 1 SGK1 expression and activity in Th17 cells. (a) SGK1 expression level based on genome-wide mRNA analysis under Th0 and Th17 conditions at 18 different time points; (b) SGK1 expression based on genome-wide mRNA analysis in WT and *Il23r*$^{-/-}$ CD4^{+} T cells stimulated with TGF-β1, IL-6 and IL-23; (c) Kinetics of SGK1 gene expression in WT or *Il23r*$^{-/-}$ CD4^{+} T cells differentiated with TGF-β1, IL-6 and IL-23. mRNA expression data are presented relative to GAPDH expression; (d, e) SGK1 kinase activity in different T cell subsets and IL-23 restimulated Th17 cells. Data are representative of three independent experiments (error bars, SD); (f) IL-23R protein-protein interaction network model. Nodes are sized proportional to their network score. Network composed of all the protein nodes with a p-value under 10^{-4}; (g) Ranked list of nodes (proteins) sorted by their score in the IL-23R network model. *P< 0.05 (Student's *t*-test).

Supplementary Fig. 2 SGK1 deficiency impairs IL-23-dependent maintenance of Th17 cells *in vitro*. (a) IL-17A and IFN-γ production from WT and *Sgk1*$^{-/-}$ memory CD4^{+} T cells differentiated under indicated Th17 differentiation conditions; (b, c) IL-17 and IFN-γ production in the supernatants from cells described in Fig. 1e, f were measured by ELISA; (d) Overlap between the *Il23r*$^{-/-}$ and *Sgk1*$^{-/-}$microarray datasets**.** Differentially expressed genes in the *Il23r*$^{-/-}$ data are compared to the differentially expressed genes in the *Sgk1*$^{-/-}$ data. Overlap is computed separately for the up- and down-regulated sets. Only significant results ($p<10^{-3}$) are presented. (e) Gene Set Enrichment Analysis

(GSEA) of the *Sgk1*$^{-/-}$ microarray data showing that WT Th17-specific genes tend to be down-regulated in *Sgk1*$^{-/-}$ Th17 cells; (f) Differentiated WT and *Sgk1*$^{-/-}$ Th17 cells were restimulated with IL-23 and expression of indicated genes was analyzed by q-PCR analysis at 4 h after stimulation with PMA and ionomycin. *P< 0.05 and **P< 0.01 (Student's *t*-test, error bars, SD). Data are representative of three independent experiments.

Supplementary Fig. 3 Impaired recall response of SGK1-deficient T cells. (a) mRNA level of SGK1 in *Cd4*^{Cre}*Sgk1*$^{+/+}$ and *Cd4*^{Cre}*Sgk1*^{flfl} CD4$^+$ T cells confirming lack of SGK1 expression in SGK1-deficient CD4$^+$ T cells. Flow cytometry analysis (b) and ELISA (c) of IL-17 and IFN-γ production by CD4$^+$ T cells isolated from immunized *Cd4*^{Cre}*Sgk1*$^{+/+}$ or *Cd4*^{Cre}*Sgk1*$^{fl/fl}$ mice and restimulated with the indicated antigens and IL-23 for 96 h. Data represents the means of two independent experiments. **P< 0.01 and ***P< 0.001 (Student's *t*-test, error bars, SD).

Supplementary Fig. 4 Impaired Th17 cell maintenance in the absence of SGK1 during EAE development. (a) IL-23R (GFP) expression on CD4$^+$ T cells isolated from the indicated organs of *Cd4*^{Cre}*Sgk1*$^{fl/fl}$*Il23r*^{gfp} or control mice at the peak of EAE; (b) EAE disease course in *Rag2*$^{-/-}$ mice adoptively transferred with control or *Il17f*^{Cre}*Sgk1*$^{fl/fl}$ CD4$^+$ T cells (n=9); (c) IL-17 production from donor CD4$^+$ cells harvested from the indicated organs 7 days after transfer (n=9); (d) CD4$^+$eYFP$^+$ T cells isolated from LN and CNS of WT and SGK1-deficient *Il17f*^{Cre}*R26R*^{eYFP} reporter mice 17 days after MOG-CFA

immunization, quantification of IL-17A production is shown as bar graph (n=10). Data are representative of three independent experiments. *P< 0.05 (Student's *t*-test).

Supplementary Fig. 5 SGK1-Foxo1 signaling axis. (a) Ranked list of nodes (proteins) sorted by their score in the SGK1 network model (Methods); (b) To detect levels of Foxo1 phosphorylation, HEK293T cells were transfected with MSCV-IRES-GFP-SGK1 and pCMV5-Foxo1 (HA) constructs and lysates were prepared. The data shows that overexpression of SGK1 increases the levels of phosphorylated Foxo1 (S256 and S319). Data are representative of two independent experiments.

Supplementary Fig. 6 Foxo1 promotes its own expression and inhibits *Il23r* expression. (a) ChIP analysis of the interaction of Foxo1 or isotype control antibody with the *Foxo1* promoter regions in WT IL-23 restimulated Th17 cells; (b) HEK293T cells were transfected with a *Foxo1* promoter-driven luciferase reporter along with the indicated plasmids and promoter activity was determined; (c) mRNA level of Foxo1 in $Cd4^{Cre}Foxo1^{fl/fl}$ $CD4^+$ T cells; (d, e) ChIP analysis of the interaction of Foxo1 (d) or RORγt (e) or isotype control antibody with the *Il23r* promoter regions in WT IL-23 restimulated Th17 cells; (f-h) HEK293T cells were transfected with a *Il23r* promoter-driven luciferase reporter along with the indicated plasmids and promoter activity was determined. Data are representative of three independent experiments.

Supplementary Fig. 7 NaCl induces and enhances expression of Th17 cell signature genes. (a) Gene Set Enrichment Analysis (GSEA) of the NaCl microarray data showing

that Th17-specific genes tend to be up-regulated in the presence of additional 40 mM NaCl; (b) mRNA expression of indicated genes in naïve WT $CD4^+$ T cells stimulated +/− 40 mM NaCl under Th0 conditions at 72 h; (c) mRNA expression of indicated genes in naïve WT $CD4^+$ T cells stimulated with 40 mM NaCl under Th17 differentiating conditions (TGF-β and IL-6) at 72 h; (d) IL-17 and IFN-γ production at 72 h in $CD4^+$ T cells differentiated in the presence of indicated cytokines +/− mannitol. $^{**}P< 0.01$ and $^{***}P< 0.001$ (Student's *t*-test, error bars, SD). Data are representative of three independent experiments.

Supplementary Fig. 8 SGK1 is essential for high salt-induced autoimmunity. (a) Representative flow cytometry plots of $CD4^+IL\text{-}17^+$ or $CD4^+IFN\text{-}\gamma^+$ T cells from the indicated organs of $Cd4^{Cre}Sgk1^{+/+}$ and $Cd4^{Cre}Sgk1^{fl/fl}$ mice fed HSD or control diet for 3 weeks; (b) Quantification of $CD4^+IL\text{-}17^+$ or $CD4^+IFN\text{-}\gamma^+$ T cells from the indicated organs of naive WT mice fed HSD or control diet for 3 weeks; (c, d) Linear-regression curves of clinical scores of EAE in $Cd4^{Cre}Sgk1^{+/+}$ and $Cd4^{Cre}Sgk1^{fl/fl}$ mice fed with HSD or control diet as in Fig. 4e; (e) Representative flow cytometry plots of $CD4^+IL\text{-}17^+$ or $CD4^+IFN\text{-}\gamma^+$ T cells from the indicated organs of $Cd4^{Cre}Sgk1^{+/+}$ and $Cd4^{Cre}Sgk1^{fl/fl}$ mice fed HSD or control diet on day 17 following immunization with MOG/CFA; (f) Intracellular cytokine production of IL-17 and IFN-γ by $CD4^+$ T cells isolated from immunized WT mice fed HSD or control diet and re-stimulated with the indicated antigens for 96 h, as determined by flow cytometry. $^{*}P< 0.05$ (Student's *t*-test). Data are representative of three independent experiments (error bars, SD).

Supplementary Table. 1 Candidate selection in the *Il23r*$^{-/-}$ and *Sgk1*$^{-/-}$ data sets.

Sheet 1 (TF analysis – IL-23R): TF that are potentially dysregulated in *Il23r*$^{-/-}$ cells. The analysis is based on significance of overlaps (p-value, column 3) between their known target genes (data sources are listed in column 2) and the differentially expressed genes. **Sheet 2 (Ranking – IL-23R network)** – ranked list of candidate genes (top 20) in *Il23r*$^{-/-}$ cells. Top table – ranking based on expression profiles. Displayed data is fold change of expression. Bottom table – ranking based on network analysis. **Sheet 3 (TF analysis - SGK1):** TF that are potentially dysregulated in *Sgk1*$^{-/-}$ cells. The analysis is based on significance of overlaps (p-value, column 3) between their known target genes (data sources are listed in column 2) and the differentially expressed genes. **Sheet 4 (Ranking - SGK1 network):** ranked list of candidate genes (top 20) in *Sgk1*$^{-/-}$ cells based on network analysis.

Supplementary Table. 2 Microarray data analysis.

Sheet 1 (Differentially expressed genes): microarray-based expression fold changes (log2) in the *Il23r*$^{-/-}$ (vs. WT during the 65-72 h segment), *Sgk1*$^{-/-}$ (vs. WT) and NaCl (vs. no treatment) datasets. Only genes that are significantly differentially expressed in at least one condition are displayed. Value of "NA" in the *Il23r*$^{-/-}$ column indicates that the respective gene was not included in the array. **Sheet 2 (Functional enrichments)**: functional enrichment analysis based on the DAVID and MsgiDB databases. In the first column (gene set), "SGK1-up" corresponds to all genes that are up-regulated in the *Sgk1*$^{-/-}$Th17 cells; "SGK1-dn" corresponds to all genes that are down-regulated in the *Sgk1*$^{-/-}$ Th17 cells; "SGK1" corresponds to all genes that are differentially expressed (either up-

or downregulated) in *Sgk1*$^{-/-}$ cells. Similar annotation is used for the NaCl data.

Experimental Procedures

Animals

C57BL/6 (B6), CD45.1, *R26R*^{eYFP}, *Rag2*$^{-/-}$ mice were purchased from Jackson Laboratory; *Cd4*^{Cre} mice were purchased from Taconic; *Il17a*^{gfp} mice were purchased from Biocytogen; *Il23r*^{gfp}, *Il23r*$^{-/-}$, *Sgk1*$^{-/-}$, *Sgk1*$^{fl/fl}$, *Foxo1*$^{fl/fl}$ and *Il17f*^{Cre} mice have been described previously [1, 2, 3, 4]. All experiments were carried out in accordance with guidelines prescribed by the Institutional Animal Care and Use Committee (IACUC) at Harvard Medical School.

Antibodies

The following antibodies were used in flow cytometry and cell sorting: CD45.2 (104, eBiosciences), CD4 (H129.19, BD Pharmingen), IL-17A (TC11-18H10.1, BD Pharmingen), IL-17F (9D3.1C8, Biolegend), IFN-γ (XMG1.2, BD Pharmingen), CD44 (IM7, Biolegend), CD62L (MEL-14, Biolegend).

Active EAE

EAE was induced using the 35–55 peptide of myelin/oligodendrocyte glycoprotein (MOG_{35-55}) as previously described [5].

In vitro T cell differentiation

Sorted naïve $CD4^+$ T cells ($CD4^+CD62L^+CD44^-$) were activated with plate-bound anti-CD3 (2 ug/ml; 145-2C11) and anti-CD28 (2 ug/ml; PV-1). The naive cells were cultured at a concentration of 2×10^6 /ml in IMDM medium supplemented with 10% FBS, L-

glutamine, HEPES, penicillin/streptomycin, gentamicin sulfate, and 2-ME. For the generation of Th17 cells, naive T cells (1×10^6/ml) were cultured with IL-6 (30 ng/ml) and TGF-β1 (3 ng/ml) on 24 well plates for 72 h. The differentiated Th17 cells (1×10^6/ml) were then transferred into blank 24 well plates in the fresh medium to rest for 72 h, following with IL-23 (20 ng/ml) restimulation in the presence of anti-CD3/28 for 72 h. IL-12 (10 ng/ml) and anti-IL-4 (10 μg/ml; 11B11) for Th1 differentiation; or IL-4 (10 ng/ml) and anti-IL-12 (10 μg/ml) for Th2 differentiation; or TGF-β1 (5 ng/ml) for Treg differentiation; IL-1β (10 ng/ml), IL-21 (50 ng/ml) for Th17 differentiation. Mouse IL-6, TGF-β1, IL-23, IL-4 and IL-12 were purchased from Miltenyi. IL-1β and IL-21 were purchased from (R&D system).

Flow cytometry

Mice were perfused with PBS before spleens, LNs and brains were harvested. Spleens and brains were pretreated with 2 μg/ml collagenase D and 1 μg/ml DNAse I (both Roche Diagnostics), and total cells were isolated by cell straining (70 μm for spleens/ 100 μm for brains). Brain homogenates were separated into neuronal and leukocyte populations by discontinuous density gradient centrifugation using isotonic Percoll (Amersham). Cells were permeablized and fixed with an intracellular staining kit (eBioscience); Annexin V/PI staining was carried out following the manufacturer's instructions (BD Biosciences). Flow cytometry was performed using a FACS Calibur (Becton Dickinson) with the antibodies listed above.

Quantitative RT-PCR

Cells were stimulated as indicated and RNA was extracted using RNeasy minikits (Qiagen). RNA expression was detected by RT-PCR with the GeneAmp 7500 Sequence Detection System or the ViiA7 Real-Time PCR System (Applied Biosystems). Expression levels were normalized to the expression of GAPDH. Primer-probe mixtures were purchased from Applied Biosystems. *Ahr* (Mm00478932-m1); *Ccr6* (Mm99999114-s1); *Foxo1* (Mm00490672-m1); *Il17a* (Mm00439619-m1); *Il17f* (Mm00521423-m1); *Il21* (Mm00517640-m1); *Il22* (Mm01226722-g1); *Il23r* (Mm00519943-m1); *Rora* (Mm01173766-m1); *Rorc* (Mm01261022-m1); *Sgk1* (Mm00441380-m1); *GAPDH* (4352339E)

Cytokine production

Sorted naïve $CD4^+$ T cells were stimulated as indicated. Cytokine concentration was determined by ELISA as previously published [6].

Western blot analysis

2-5 x 10^6 cells were lysed in whole cell extract buffer (50 mM Tris-HCl, pH 7.5, 150 mM NaCl, 0.5% Igepal CA-630, 0.2 mM EDTA, 10 mM Na2VO4, 10% glycerol, protease inhibitors) to obtain whole cell lysates. Alternatively, nuclear lysates were prepared with a nuclear extract kit following the manufacturer's instructions (Active Motif). Proteins were separated by SDS-PAGE gel electrophoresis using 4-12% NuPAGE Bis-Tris gels (Invitrogen) followed by transfer to nitrocellulose membrane. To block unspecific binding, membranes were incubated with 5% milk in TBST (0.5 M NaCl, Tris-HCl, pH 7.5, 0.1% (v/v) Tween-20) for 60 min and washed once with TBST. Proteins of interest

were detected by incubating membranes over night at 4°C in 5% BSA/TBST with the indicated antibodies (listed below), washing with TBST three times 10 min and incubating with horseradish peroxidase–conjugated anti-rabbit or anti-mouse antibody (Cell Signaling, 7074 and 7076). Bound antibody was detected by using Immobilon Western chemiluminescent HRP substrate (Millipore). Antibodies used for Western blot analysis: anti-Foxo1 (Cell Signaling, 2880), anti-p-Foxo1 (S256) (Cell Signaling, 9461), anti-p-Foxo1 (S319) (Santa Cruz, sc-23771R), anti-SGK (Cell Signaling, 3272), anti-HA tag (C29F4, Cell Signaling), anti-β-Actin (Santa Cruz, sc-47778), anti-β-Tubulin (AA2, Millipore), anti-Histone H3 (3H1, Cell Signaling).

Immunoprecipitation

Cell lysates were prepared as described above and proteins were immunoprecipitated by incubation of lysates with 3 μg antibody (listed below) over night at 4°C and pull-down of antibody-protein precipitates with Dynabeads Protein G (Invitrogen). Beads were washed extensively and proteins eluted with NuPAGE LDS sample buffer (10% β-mercaptoethanol). The presence of immuncomplexed proteins was determined by Western blot analysis with the antibodies listed. Rabbit polyclonal anti-Foxo1 (ab39670, Abcam), mouse monoclonal anti-Foxo1 (C-9, Santa Cruz), rat monoclonal anti-RORγt (B2D, eBioscience), rabbit polyclonal anti-RORγt (H-190, Santa Cruz).

Kinase activity assay

Sorted naïve WT T cells were differentiated *in vitro*, as described above. Different T cell subsets were analysed 3 days after stimulation, whereas restimulated Th17 cells were

differentiated towards Th17 cells for 3 days, rested for 3 days and analysed after restimulation with IL-23 for 1 h. Cell lysates were prepared as described above and SGK1 was immunoprecipitated from the lysates with anti-SGK1 (Abcam, ab43606). The immunoprecipitate was washed extensively and SGK1 kinase activity was assessed with a luminescence-based assay (SGK1 kinase ADP-Glo™ Kinase Assay, Promega).

Plasmids

Murine SGK1 was cloned from pCMV-Sport6 (Openbiosystems, MMM1013-64329) into the MSCV-IRES-GFP vector at EcoRI and XhoI sites.

Reporter assays

HEK 293T cells (4 x 10^4 cells/well, 48 well plate) were transiently transfected with the indicated expression vectors, empty vector controls as well as the promoter Firefly luciferase-reporter constructs and Renilla luciferase reporter vector (Promega) with Fugene HD (Roche). 48 h after transfection, luciferase expression was determined by measuring luminescence with the Dual-Luciferase Reporter Assay System (Promega). The Firefly luciferase activity was normalized to Renilla luciferase activity. Data is representative of at least two independent experiments; each data point represents duplicate values. The following vectors were used; MSCV-IRES-GFP-SGK1, MSCV-IRES-GFP-RORγt (kind gift of Dr. Liang Zhou), pCMV5-Foxo1 (kind gift of Domenico Accili, Addgene, plasmid 12142), pCMV5-Foxo1AAA (kind gift of Domenico Accili, Addgene, plasmid 17547) pGL3-Foxo1 reporter (kind gift of Dr. Jean-Baptiste Demoulin), pTA-Luc IL23R reporter (kind gift of Dr. Kojiro Sato),

ChIP PCR

Naïve T cells were treated with the indicated cytokines. ChIP was performed according to manufacturer's instructions (Cell Signaling) and samples were analyzed by SYBR Green real-time PCR (primers described below). The following antibodies were used for ChIP: anti-Foxo1 (Abcam, ab39670), anti-RORγt (eBioscience, AFKJS-9).

Microarray data

Naïve T cells were isolated from WT and *Il23r*$^{-/-}$ mice, and were treated with IL-6, TGF-β1 and IL-23. Affymetrix microarray HT_MG-430A was used to measure the resulting mRNA levels at four different time points (49 h, 54 h, 65 h, 72 h).

As an additional dataset for generating the candidate list in Figure 1a we used gene expression profiles from WT naïve T cells treated with IL-6 and TGF-β1 (the generation of the list is explained in detail below). This data was collected from 18 time points (30 min to 72 h) using the Affymetrix microarray HT_MG-430A. As control, we used WT Th0 cells harvested at the same time points.

Th17 cells from WT and *Sgk1*$^{-/-}$ mice were restimulated with IL-23. Affymetrix microarray Mouse430_2 was used to measure the resulting mRNA levels in duplicate. For the analysis of the NaCl effect, naïve T cells were isolated from WT mice, and placed under Th0 conditions with or without 40 mM NaCl for 72 h. The resulting mRNA levels were then measured in duplicate with Affymetrix microarray Mouse430_2.

Expression data was preprocessed using the RMA algorithm followed by quantile normalization, using the default parameters in the ExpressionFileCreator module of the GenePattern suite [7].

Detection of differentially expressed genes

Genes that are differentially expressed in the *Il23r*$^{-/-}$ time course (compared to the WT time course) were found using three methods: **(1)** Fold change, reporting all genes that had more than 2-fold change (up or down) compared to the control sample during at least two time points. **(2)** Polynomial fit. We used the EDGE software [8], which was designed for identifying differential expression in time course data. We set a threshold of q-value <=0.01. **(3)** Sigmoidal fit. Using an algorithm similar to [8]. However, instead of polynomials we used a sigmoid function [9], which were recently observed as more adequate for modeling time course gene expression data. As above, we set a threshold of q-value <=0.01.

We defined all genes that pass at least two out of the three tests as differentially expressed. The reported fold change levels in Fig. 1h and Table S2 are the average over the last two time points (65 h, 72 h). To avoid spurious fold levels due to low expression values a small constant was added to the expression values (c=50). Collapsing of probesets into genes is done in the following way: for differentially expressed genes the average over all differentially expressed probesets was used. For other genes we used the probeset with the highest absolute expression level.

To find genes that are differentially expressed in the NaCl conditions or in *Sgk1*$^{-/-}$ cells (compared to the respective control) we computed fold changes between the expression levels of each probeset in the case and control conditions. To avoid spurious fold levels due to low expression values we added a small constant to the expression values as above. We only reported cases where more than 50% of the four possible case-control comparisons were over a cutoff of 1.5 fold change. As an additional filter, we computed a Z-score by comparing the mean of the expression levels in the case samples to the control samples. We only reported cases with a corresponding p-value lower than 0.05. We collapsed probesets into genes as above.

Overlap between the *Il23r*$^{-/-}$ and *Sgk1*$^{-/-}$ microarray datasets

We used the Fisher exact test to compare the list of differentially expressed genes in the *Il23r*$^{-/-}$ data and the differentially expressed genes in the *Sgk1*$^{-/-}$ data. Overlap was computed separately for the up- and down-regulated sets (4 combinations altogether; see Supplementary Fig. 2d).

Generating the candidate list for the *Il23r*$^{-/-}$ data

We ranked the genes based on the average of: **(1)** Average fold increase during the time segment (48-72 h), comparing WT naïve T cells treated with IL-6 and TGF-β1 to Th0 cells. **(2)** Average fold decrease during the time segment (65-72 h), comparing *Il23r*$^{-/-}$ and WT cells treated with IL-6, TGF-β1, and IL-23.

Network analysis of the *Il23r*$^{-/-}$ T cell data

We collected protein-protein interaction (PPI) data from several public databases ([10, 11, 12, 13], http://www.netpath.org/, and http://www.phosphosite.org/). Interactions from [10, 12, 13] are assigned with a confidence value in the range of [0…1], according to the experimental evidence that supports them as in [14]. Interactions from the SPIKE database [11] are assigned with a score using the confidence classification provided in the database. Specifically, the four confidence classes (from high to low) were associated with the confidence levels at the 10-th, 6-th, 3-rd, and 1-st quantile. Interactions from the curated databases PhosphoSite and NetPath were assigned a maximal confidence score of 1. Since most interactions are in humans, we used orthology mapping to transfer the interaction data to mice.

Based on manual literature curation, we collected a set of genes that are known to play a role in IL-23R signaling (termed the "IL-23R signaling set"). Those include: *Il23r, Il12rb1, Tyk2, Jak2, Akt1, Pik3r1, Pdk1, Stat3, Stat4*, and *Nfkbib*. We then used an in-house command line version of the ANAT software [14] for finding a PPI network that connects the IL-23R signaling set to the set of transcription factors (TF) whose activity is dysregulated under *Il23r*$^{-/-}$ (see next section for the identification of these responsive TF).

We considered several variations on the default application of ANAT: **(1)** Using only post-translational modifications (instead of all the PPI data available). **(2)** Penalizing high degree nodes (thus avoiding unspecific, and potentially irrelevant hub nodes). Here, we

set the curvature parameter to be 2 (i.e. the penalty is proportional to the square root of the degree). The dominance parameter is set such that the average node weight is equal to the average edge weight. **(3)** Introducing a bias, preferring genes that are differentially expressed in *Il23r*$^{-/-}$ cells. Here we assigned a prior confidence value of 1 to the differentially expressed genes, and a value of 0.5 to the remaining genes.

For a robust analysis, we applied ANAT using all eight possible "yes/no" combinations of these three variations. Each node in each of the eight resulting networks is associated with a p-value, denoting the probability for it to be included in the network by chance. For a given network and for each node with a p-value lower than 10^{-4}, we computed a centrality score (as in [14]) defined as the number of downstream TF whose path to the IL-23R signaling set passes through that node. Nodes that are not included in the network or have a p-value above the cutoff are associated with a centrality score of zero. We then reported the average score over all eight network configurations.

Network analysis of the *Sgk1*$^{-/-}$ T cell data

We utilized a similar analysis as above. ANAT was applied for finding a PPI network that connects SGK1 to the set of TF whose activity is dysregulated in *Sgk1*$^{-/-}$ cells (see next section for the identification of these responsive TF). As above, we computed eight different configurations. For the third variation (introduction of node bias) we used the genes that are differentially expressed in *Sgk1*$^{-/-}$ cells.

Identification of responsive TF in the *Sgk1*$^{-/-}$ T cell data

We identified TF that are potentially dysregulated in *Sgk1*$^{-/-}$ cells by looking for significant overlaps between their known target genes and the differentially expressed genes. TF-target interaction data was obtained from public databases [15, 16, 17, 18, 19, 20]. Additional potential interactions, were obtained by applying the SPC clustering algorithm [21] to data from the mouse ImmGen consortium (http://www.immgen.org; January 2010 release; [22]), which includes 484 microarray samples from 159 cell subsets from the innate and adaptive immune system of the mouse. For every TF in our database we computed the statistical significance of its overlap with the set of differentially expressed genes using the Fisher exact test. We reported cases with $p< 5\times10^{-5}$ and fold enrichment > 1.5.

We used two additional sources for the TF analysis: **(1)** a statistical analysis of binding-site enrichment in promoter regions that are associated with the differentially expressed genes using the PRIMA algorithm [23]. **(2)** The TF enrichment module of the commercial IPA software (http://www.ingenuity.com/). As above, we used a cutoff of $p <5\times10^{-5}$.

Identification of responsive TF in the *Il23r*$^{-/-}$ T cell data

The analysis of the *Il23r*$^{-/-}$ T cell data uses a similar strategy as the one applied to the *Sgk1*$^{-/-}$ T cell data. However, instead of only crossing the TF databases with the entire set of differentially expressed genes, we also used smaller clusters of genes that have similar temporal expression characteristics. We considered several ways for grouping the differentially expressed genes, based on their time course expression data: **(1)** For each time point, group all the genes that are over- or under-expressed during that time. **(2)** For each time point, group all the genes that showed a significant change in their expression

(increase/ decrease) as compared with the previous time point. **(3)** Cluster the genes based on their profiles under the knockout condition. We use k-means clustering with the minimal k such that the within cluster similarity (average pearson correlation with centroid) is higher than 0.75 for all clusters. **(4)** Cluster the genes based on a concatenation of their knockout profile and their WT profile (using k-means as before).

T cell subset signature genes

We downloaded and analyzed the gene expression data from [24] and pre-processed it using the RMA algorithm followed by quantile normalization, using the default parameters in the ExpressionFileCreator module of the GenePattern suite [7]. This data includes duplicate microarray measurements from Th17, Th1, Th2, iTreg, nTreg, and naïve $CD4^+$ T cells. For a given cell subset we evaluated for each gene whether it is over-expressed compared to all other cell subsets using a one-sided t-test. We retained all cases that had a p-value under 0.05. As an additional filtering step, we required that that the expression level of the gene in the given cell subset is at least 1.25 fold higher than its expression in all other cell subsets. As before, to avoid spurious fold levels due to low expression values we added a small constant to the expression values (c=50). We evaluated the overlap between differentially expressed genes (in either *Sgk1*$^{-/-}$ or NaCl-treated cells) and the subset-specific genes using Fisher exact test. As an additional test, we performed GSEA analysis [19] testing the correlation between the different T cell subsets and the fold change of genes in either *Sgk1*$^{-/-}$ or NaCl-treated cells. In this analysis, for a given T-cell subset, the "gene set" is the list of genes that are up-regulated in the subset; and the expression data set is the log-expression fold change.

Functional enrichment analysis

We used two sources for the functional enrichment test for the genes that are differentially expressed in either *Sgk1*$^{-/-}$ or NaCl-treated cells: **(1)** The DAVID functional annotation tool [25]; **(2)** The MsigDB database [19], using the "canonical pathway" subset of the curated gene set (c2.cp.v3.0), the "cellular process" subset of the Gene ontology gene set (c5.all.v3.0), and the motif gene set (c3.all.v3.0). We evaluate the significance of the MsigDB overlaps using the Fisher exact test.

Statistical analysis

Statistical analysis was performed using GraphPad Prism (GraphPad Software Inc., La Jolla, CA). The data were analyzed by a paired sign *t*-test or Student's *t*-test. All *P* values of 0.05 or less were considered statistically significant.

Sequences of primers used in chromatin immunoprecipitation (ChIP) assay

Foxo1 promoter 1 s	GAGTCAGGATCCCCAGACAA
Foxo1 promoter 1 as	AGACAGAAGAGGGCAGCAGA
Foxo1 promoter 2 s	GGCCAATGCTCTGCTACAAT
Foxo1 promoter 2 as	CCTGCAAGTTCAGGTGAGGT
Foxo1 promoter 3 s	TGTATCCCCTGCATCCTCA
Foxo1 promoter 3 as	TGGCAATGTTCTATTTCCTAAGGT
Foxo1 promoter 4 s	TTCACAGCTGGATTTCATCG
Foxo1 promoter 4 as	ATGGATGAGCCTAAGCAGGA
Foxo1 promoter 5 s	CGGTTTGCCTCCTAGCAAT
Foxo1 promoter 5 as	AGGCGGCAGTAGGTTGGT
Foxo1 promoter 6 s	ATGTATTAAATTGTTTTTCTCCTTGG
Foxo1 promoter 6 as	TGTCAAGCATCTATCTACTCCTCTG
Il23r promoter 1 s	AAGTTGGAGGCAGGGACATCAAGA
Il23r promoter 1 as	TGCTTGGCTTCTAGTTGGTGGACT
Il23r promoter 2 s	AGCCAGTACAGGAACCACAAGGAA
Il23r promoter 2 as	ACAAATGCCAAGAGGAGACAGGGA
Il23r promoter 3 s	TAGGGTTGGGAAATGAGGCTGACA
Il23r promoter 3 as	AAGGAGTGCAAGAGGAGCATTGGA
Il23r promoter 4 s	TGAAGCTTGGACACCAAGAGTCCT
Il23r promoter 4 as	TCTAGGCCAGGTGGTGGTTTGAAT
Il23r promoter 5 s	TCTCTCGTACTGCCAATTGCACCT
Il23r promoter 5 as	AGGCAGCACAAGCTGTAGAATTGC
Il23r promoter 6 s	AGAGTAGCTGCCTGATGAAGGACA
Il23r promoter 6 as	TTGAGCAGAGCATCAGGGTGGAAT

References:

1. Ouyang W, Beckett O, Ma Q, Paik JH, DePinho RA, Li MO. Foxo proteins cooperatively control the differentiation of Foxp3+ regulatory T cells. *Nature immunology* 2010, **11**(7)**:** 618-627.

2. Petermann F, Rothhammer V, Claussen MC, Haas JD, Blanco LR, Heink S, *et al.* gammadelta T cells enhance autoimmunity by restraining regulatory T cell responses via an interleukin-23-dependent mechanism. *Immunity* 2010, **33**(3)**:** 351-363.

3. Croxford AL, Kurschus FC, Waisman A. Cutting edge: an IL-17F-CreEYFP reporter mouse allows fate mapping of Th17 cells. *J Immunol* 2009, **182**(3)**:** 1237-1241.

4. Fejes-Toth G, Frindt G, Naray-Fejes-Toth A, Palmer LG. Epithelial Na+ channel activation and processing in mice lacking SGK1. *Am J Physiol Renal Physiol* 2008, **294**(6)**:** F1298-1305.

5. Stromnes IM, Goverman JM. Active induction of experimental allergic encephalomyelitis. *Nat Protoc* 2006, **1**(4)**:** 1810-1819.

6. Jager A, Dardalhon V, Sobel RA, Bettelli E, Kuchroo VK. Th1, Th17, and Th9 effector cells induce experimental autoimmune encephalomyelitis with different pathological phenotypes. *J Immunol* 2009, **183**(11)**:** 7169-7177.

7. Reich M, Liefeld T, Gould J, Lerner J, Tamayo P, Mesirov JP. GenePattern 2.0. *Nat Genet* 2006, **38**(5)**:** 500-501.

8. Storey JD, Xiao W, Leek JT, Tompkins RG, Davis RW. Significance analysis of time course microarray experiments. *Proceedings of the National Academy of Sciences of the United States of America* 2005, **102**(36)**:** 12837-12842.

9. Chechik G, Koller D. Timing of gene expression responses to environmental changes. *J Comput Biol* 2009, **16**(2)**:** 279-290.

10. Breitkreutz BJ, Stark C, Reguly T, Boucher L, Breitkreutz A, Livstone M, *et al.* The BioGRID Interaction Database: 2008 update. *Nucleic Acids Res* 2008, **36**(Database issue)**:** D637-640.

11. Elkon R, Vesterman R, Amit N, Ulitsky I, Zohar I, Weisz M, *et al.* SPIKE--a database, visualization and analysis tool of cellular signaling pathways. *BMC Bioinformatics* 2008, **9:** 110.

12. Peri S, Navarro JD, Amanchy R, Kristiansen TZ, Jonnalagadda CK, Surendranath V, *et al.* Development of human protein reference database as an initial platform for approaching systems biology in humans. *Genome Res* 2003, **13**(10)**:** 2363-2371.

13. Xenarios I, Salwinski L, Duan XJ, Higney P, Kim SM, Eisenberg D. DIP, the Database of Interacting Proteins: a research tool for studying cellular networks of protein interactions. *Nucleic Acids Res* 2002, **30**(1)**:** 303-305.

14. Yosef N, Zalckvar E, Rubinstein AD, Homilius M, Atias N, Vardi L, *et al.* ANAT: a tool for constructing and analyzing functional protein networks. *Sci Signal* 2011, **4**(196)**:** pl1.

15. Linhart C, Halperin Y, Shamir R. Transcription factor and microRNA motif discovery: the Amadeus platform and a compendium of metazoan target sets. *Genome Res* 2008, **18**(7)**:** 1180-1189.

16. Zheng G, Tu K, Yang Q, Xiong Y, Wei C, Xie L, *et al.* ITFP: an integrated platform of mammalian transcription factors. *Bioinformatics* 2008, **24**(20)**:** 2416-2417.

17. Wilson NK, Foster SD, Wang X, Knezevic K, Schutte J, Kaimakis P, *et al*. Combinatorial transcriptional control in blood stem/progenitor cells: genome-wide analysis of ten major transcriptional regulators. *Cell Stem Cell* 2010, **7**(4)**:** 532-544.

18. Lachmann A, Xu H, Krishnan J, Berger SI, Mazloom AR, Ma'ayan A. ChEA: transcription factor regulation inferred from integrating genome-wide ChIP-X experiments. *Bioinformatics* 2010, **26**(19)**:** 2438-2444.

19. Liberzon A, Subramanian A, Pinchback R, Thorvaldsdottir H, Tamayo P, Mesirov JP. Molecular signatures database (MSigDB) 3.0. *Bioinformatics* 2011, **27**(12)**:** 1739-1740.

20. Jiang C, Xuan Z, Zhao F, Zhang MQ. TRED: a transcriptional regulatory element database, new entries and other development. *Nucleic Acids Res* 2007, **35**(Database issue)**:** D137-140.

21. Blatt M, Wiseman S, Domany E. Superparamagnetic clustering of data. *Phys Rev Lett* 1996, **76**(18)**:** 3251-3254.

22. Heng TS, Painter MW. The Immunological Genome Project: networks of gene expression in immune cells. *Nature immunology* 2008, **9**(10)**:** 1091-1094.

23. Elkon R, Linhart C, Sharan R, Shamir R, Shiloh Y. Genome-wide in silico identification of transcriptional regulators controlling the cell cycle in human cells. *Genome Res* 2003, **13**(5)**:** 773-780.

24. Wei G, Wei L, Zhu J, Zang C, Hu-Li J, Yao Z, *et al.* Global mapping of H3K4me3 and H3K27me3 reveals specificity and plasticity in lineage fate determination of differentiating CD4+ T cells. *Immunity* 2009, **30**(1)**:** 155-167.

25. Huang da W, Sherman BT, Lempicki RA. Systematic and integrative analysis of large gene lists using DAVID bioinformatics resources. *Nat Protoc* 2009, **4**(1)**:** 44-57.